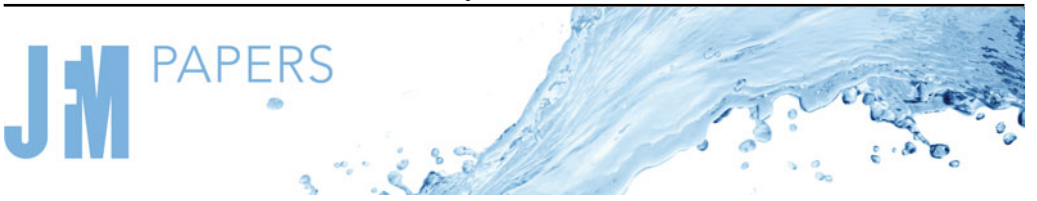
J. Fluid Mech. (2026), *vol.* 1034, A18, doi:10.1017/jfm.2026.11447



Water waves over a compressible muddy seabed

Linlong Tong[1,2], **Jisheng Zhang**[1,2], **Jinhai Zheng**[1,2], **Yakun Guo**[3] and **Ning Chen**[2]

[1]Key Laboratory of Ministry of Education for Coastal Disaster and Protection, Hohai University, Nanjing 210098, PR China

[2]College of Harbor, Coastal and Offshore Engineering, Hohai University, Nanjing 210098, PR China

[3]Faculty of Engineering and Informatics, University of Bradford, Bradford BD7 1DP, UK

Corresponding author: Jisheng Zhang, jszhang@hhu.edu.cn

(Received 29 November 2025; revised 2 February 2026; accepted 16 March 2026)

An asymptotic theory is developed to investigate the interaction of surface water waves and a compressible muddy seabed in water of intermediate depth. The water column is treated as inviscid outside a thin bottom boundary layer, the thickness of which is assumed to be of the same order of magnitude as the wave amplitude. The seabed is modelled as an isotropic and homogeneous poro-viscoelastic layer with an incompressible solid skeleton and a compressible pore fluid. The thickness of the seabed is assumed to be comparable to the wave amplitude. Using a perturbation approach, the leading-order analytical solutions for the wave and mud flow are derived, while the evolution of the wave envelope, the mean Eulerian velocity and the mass transport velocity beneath progressive waves are obtained at the second order. Based on the present solution, the wave motion and the induced mass transport are analysed and compared with previous solutions that ignore the compressibility of the seabed. The results demonstrate that the compressibility of the seabed plays a critical role in modulating the flows within both the seabed and the overlying bottom boundary layer. Neglecting compressibility may lead to an underestimation of the interface vertical displacement in highly elastic beds and an overestimation in viscous-dominated cases. Consequently, the Reynolds stress distributions in these regions deviate significantly from predictions based on incompressible seabed theory. This inaccuracy further propagates to the prediction of second-order steady currents and mass transport velocities.

Key words: coastal engineering, mass transport, viscoelasticity

1. Introduction

Cohesive particles are commonly transported by inland rivers into estuaries, where they subsequently deposit along coastal regions to form cohesive seabeds (Talling, Baker &

© The Author(s), 2026. Published by Cambridge University Press.

https://doi.org/10.1017/jfm.2026.11447 Published online by Cambridge University Press

Pope 2022). These seabeds are widely observed in numerous coasts and estuaries worldwide, including the Yellow Sea coastlines between China and Korea (Healy, Wang & Healy 2002; Garnier, Huang & Mei 2013), the South China Sea coasts (Liu *et al.* 2023), the Indian Ocean coast of South Africa (Winterwerp *et al.* 2007), the Kerala coast in southwest India (Mathew, Baba & Kurian 1995; Samiksha *et al.* 2017) and coastal areas of South America (Gade 1958; Yamamoto 1981). Laboratory and field observations have demonstrated that when water waves propagate over cohesive seabeds, the seabed experiences periodic shear stress and dynamic pressure at the water–seabed interface, which can lead to the resuspension of cohesive particles into the water column or seabed liquefaction, forming a thin muddy layer (Mathew *et al.* 1995; Sumer 2014*a*; Liu *et al.* 2022). This thin muddy layer plays an important role in wave dynamics (Ng 2004; Tong *et al.* 2020; Chen *et al.* 2026). For example, as reported by Elgar & Raubenheimer (2008), wave energy dissipates by 70 % over a propagation distance of 1.8 km across the muddy seabed on the Louisiana continental shelf. In addition, internal flows within the seabed induced by wave motion are important in determining the transport of sediment and pollutants in coastal regions (Piedra-Cueva 1995; Ng & Zhang 2007; Ji *et al.* 2026; Zhao *et al.* 2026).

Mud in different locations can exhibit distinct rheological behaviours, primarily due to variations in its chemical composition and sediment concentration (Chan & Liu 2009). Given the wide range of seafloor properties, the interaction between surface water waves and a muddy seabed has been extensively modelled using a two-layer system, where the mud layer is represented by various constitutive relations. The pioneering work of Dalrymple & Liu (1978) introduced the viscous fluid model, establishing a comprehensive theoretical framework for wave attenuation over a laminar viscous mud layer. This model successfully accounted for the high damping rates observed in field measurements (Gade 1958) and was subsequently extended via asymptotic analyses for cases in which the mud layer thickness is comparable to that of the Stokes boundary layer (Ng 2000; Liu & Chan 2007*a*). To capture the solid-like behaviour of more consolidated sediments, elastic (Wen & Liu 1995*a*) and viscoelastic models (Macpherson 1980; Liu & Chan 2007*b*) were developed. These studies demonstrated that viscoelasticity could significantly modify wave dispersion characteristics and, under certain conditions, induce resonant wave–mud interactions that enhanced energy dissipation by several orders of magnitude (Maa & Metha 1990; Piedra-Cueva 1993; Chan 2022). Moreover, to represent the yield stress exhibited by fluid mud, viscoplastic models such as the Bingham plastic model were employed (Mei & Liu 1987; Park & Liu 2010). Such models predict the formation of fluidised mud layers and the development of alternating plug and shear flow zones under wave-induced cyclic loading (Chan & Liu 2009), revealing a complex rheological response that extends beyond that of a simple Newtonian fluid.

Critically, rheological experiments on natural mud under oscillatory shear conditions have consistently revealed viscoelastic behaviour with frequency-dependent material properties (Jiang & Mehta 1995; Huang & Huhe 2009; Xu & Huhe 2016), highlighting the limitations of models relying on constant rheological parameters. Although these linear and nonlinear constitutive models have significantly advanced our understanding of the first-order wave dynamics, including wave dispersion, attenuation and the resulting oscillatory mud motion (Ziebell, Farina & Korotov 2018; Tong *et al.* 2026*a*), their applicability remains largely restricted to primary harmonic responses (Liu & Chan 2007*b*; Ng & Zhang 2007; Mei *et al.* 2010).

During wave propagation, a small mass transport velocity, comprising two components, i.e. the mean Eulerian velocity and the Stokes drift velocity, can be generated in the

https://doi.org/10.1017/jfm.2026.11447 Published online by Cambridge University Press

water column and seabed (Mei *et al.* 2005). The foundational theory for mass transport in a wave boundary layer over a rigid, impermeable bed was established by Longguet-Higgins (1953). This framework was subsequently extended to more complex, permeable or deformable seabeds. Dore (1970) first investigated mass transport in a two-layer viscous system, demonstrating that the drift velocity could exceed that of a single-layer system by an order of magnitude due to intense interfacial shear. However, these early studies neglected viscous damping and were limited to pure progressive or standing waves in closed systems. Subsequent research has systematically incorporated the effects of seabed properties on mass transport. For a rigid porous bed, experimental and theoretical studies showed that permeability could enhance the mean Eulerian velocity within the wave boundary layer Liu, Davis & Downing (1996), and the Lagrangian drift could be generated within the seabed (Weber & Ghaffari 2023).

For muddy seabeds, rheology becomes paramount. Wen & Liu (1995*a*) derived analytical solutions for the mass transport velocity within the boundary layer adjacent to a purely elastic seabed and in the core region of the water column, showing that the mass transport velocity above a soft elastic bed could be twice that over a rigid bed in shallow water. Based on viscous fluid models, Wen & Liu (1995*b*) investigated the effects of viscous damping on mass transport velocity in a two-layer fluid system. It was found that the resulting mass transport velocity profiles differed significantly from those obtained by Dore (1970), who neglected viscous attenuation. Similarly, Piedra-Cueva (1995) derived expressions for the mass transport velocity of spatially decaying waves by solving the momentum and continuity equations in the Lagrangian coordinate system. Two distinct physical scenarios were analysed: the first involved waves in a closed channel and the second considered waves in an unbounded domain, where the steady-state mass flux might be non-zero. Subsequently, under the assumption that the muddy seabed was thin, asymptotic solutions for the mass transport velocity in the two-layer system were obtained by Ng (2000, 2004) for progressive and partially standing waves. The theories based on viscous fluid models for mud provided a baseline for predicting mass transport within the mud layer, however, some experiments revealed quantitative discrepancies compared with these model predictions, highlighting the important influence of more complex rheological behaviours (Sakakiyama & Byker 1989; Park & Liu 2010). Therefore, an analytical theory was developed by Ng & Zhang (2007) for the mass transport induced by a progressive wave propagating in water over a thin layer of viscoelastic mud. Garnier *et al.* (2013) further investigated the steady current generated by nonlinear waves propagating over a viscoelastic muddy beach and found that the steady current might in turn cause non-uniform thickening of the mud layer.

As mentioned above, wave motion over a muddy seabed and the induced mud flows have been extensively studied in the past decades. All those studies are based on the assumption that the seabed is fully saturated and incompressible. However, in the field the muddy seabeds in coastal regions are often not fully saturated. For example, the degree of saturation of mud is 0.9 at a water depth of 12.5 m in the Mississippi Delta and 0.89 at a depth of 9 m in the Yellow River Delta (Yamamoto 1981; Song *et al.* 2022). Although field observations indicate that seabeds are highly saturated, the apparent bulk modulus of elasticity of the pore fluid decreases drastically even when the pore water contains a very small amount of air. For instance, it decreases by four orders of magnitude when the saturation degree of soil is reduced from 1 to 0.95 under atmospheric pressure (Yamamoto *et al.* 1978). Consequently, the bulk modulus of elasticity of the pore fluid becomes comparable to the shear modulus of the mud (Yamamoto 1981), indicating that the mud behaves as a compressible medium. Moreover, theoretical and experimental

https://doi.org/10.1017/jfm.2026.11447 Published online by Cambridge University Press

studies demonstrate that the compressibility of seabed soil plays a significant role in bed deformation (Yamamoto *et al.* 1978; Tong & Liu 2022) and wave propagation (Liu, Park & Lara 2007; Korde 2024), suggesting that flow dynamics cannot be adequately explained under the assumption of an incompressible seabed. Recently, Abdolali, Kirby & Bellotti (2015) proposed a depth-integrated equation to investigate the propagation and dissipation of hydro-acoustic waves in a weakly compressible ocean overlying a weakly compressible viscous sediment layer. Subsequently, Abdolali, Kadri & Kirby (2019) clarified the influence of compressibility (both in the water column and the elastic seabed) on the phase speed and arrival times for long waves. However, the influence of seabed compressibility on wave motion and mass transport in coastal regions remains unclear. To address this knowledge gap, a new asymptotic theory is developed in this study to investigate wave propagation in water of intermediate depth over a compressible muddy seabed.

In the present work, a theoretical framework is formulated to describe surface wave propagation over a thin, compressible muddy seabed. The water column is divided into an inviscid core and a thin wave boundary layer, the latter having a thickness comparable to the wave amplitude. The seabed is modelled as an isotropic and homogeneous poro-viscoelastic medium (Sumer 2014*b*). Based on the two-phase model, the pore fluid is assumed to be compressible, while the mud's solid skeleton is treated as incompressible. By employing a perturbation approach, leading-order analytical solutions for the wave field and mud motion are derived. At second order, the analysis yields the evolution of the wave envelope, the mean Eulerian velocity and the mass transport velocity under progressive waves. This model provides a more realistic representation of wave–seabed interactions by explicitly accounting for pore-fluid compressibility, thereby offering improved insight into the mechanisms governing wave attenuation and sediment transport in cohesive marine environments.

The remainder of this paper is organised as follows. The governing equations and boundary conditions for the motions of water waves, pore fluid and the soil skeleton are presented in § 2. In § 3 the scales of the dimensionless parameters involved in these equations and conditions are analysed, and the fundamental assumptions are established. In § 4 a multiple-scale perturbation analysis is formulated to investigate the coupled wave–mud dynamics, accounting for the irrotational core flow in the water column, the rotational shear flow within the seabed and bottom boundary layer, and the resulting mass transport. In § 5 the leading-order boundary value problems for wave motion and mud flow are solved; the second-order boundary value problems, concerning the evolution of the wave envelope, wave-induced steady currents and mass transport velocity, are addressed in § 6. In § 7 the wave motion and the induced mass transport are investigated based on the present solution and compared with previous solutions that ignore the compressibility of the seabed. Finally, concluding remarks are provided in § 8.

2. Governing equations and boundary conditions

As shown in figure 1, we consider a train of water waves with surface displacement, $\eta'(x', t')$, characteristic amplitude, A, frequency, ω, and wavenumber, k', propagating in a constant water depth, h', over a layer of mud with a constant thickness, d. The mud is modelled as a poro-viscoelastic medium, with effective dynamic viscosity, μ, permeability, k_s, shear modulus, G, and porosity, n. Under the wave loading, the water and mud interface oscillates with a displacement, ζ', and characteristic amplitude, b. The Cartesian coordinates (x', z') are used on the vertical plane, originating at the still water

https://doi.org/10.1017/jfm.2026.11447 Published online by Cambridge University Press

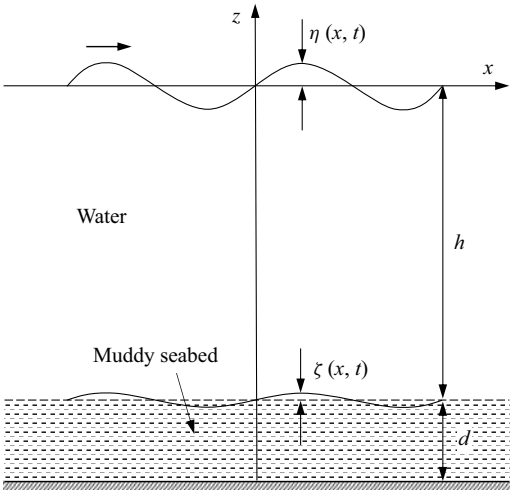


Figure 1. Sketch of water waves propagating over a muddy seabed.

level. In the analysis, the following normalisations are introduced:

$$\left.\begin{aligned} &x=\frac{\omega^2}{g}x', \quad z=\frac{\omega^2}{g}z', \quad k=\frac{g}{\omega^2}k', \quad t=\omega t', \quad \eta=\frac{\eta'}{A},\\ &p=\frac{1}{\rho g A}p', \quad (u,\,w)=\frac{1}{A\omega}(u',\,w'), \quad \Phi=\frac{\omega}{gA}\Phi', \end{aligned}\right\} \tag{2.1}$$

for the wave motion, and

$$\left.\begin{aligned} &x=\frac{\omega^2}{g}x', \qquad Z=\frac{z'+h'+d}{d}, \qquad \zeta=\frac{\zeta'}{\epsilon A}, \qquad t=\omega t',\\ &U=\frac{U'}{A\omega}, \quad \mathscr{U}=\frac{\mathscr{U}'}{A\omega}, \quad W=\frac{A}{d}\frac{W'}{\epsilon A\omega}, \quad \mathscr{W}=\frac{A}{d}\frac{\mathscr{W}'}{\epsilon A\omega}, \quad P=\frac{1}{\rho g A}P',\\ &\tilde{\boldsymbol{\tau}}_{ij}=\frac{d}{\mu_w A\omega}\tilde{\boldsymbol{\tau}}'_{ij}, \quad \boldsymbol{\tau}_{ij}=\frac{d}{\mu A\omega}\boldsymbol{\tau}'_{ij}, \quad \tilde{\boldsymbol{\varepsilon}}_{ij}=\frac{d}{A\omega}\tilde{\boldsymbol{\varepsilon}}'_{ij}, \quad \boldsymbol{\varepsilon}_{ij}=\frac{d}{A\omega}\boldsymbol{\varepsilon}'_{ij}, \end{aligned}\right\} \tag{2.2}$$

for the muddy flow, where ρ is the density of water, g denotes the acceleration of gravity, k indicates the wavenumber, p represents the dynamic water pressure, Φ is the velocity potential in the water layer, P indicates the dynamic pressure inside the mud, $\boldsymbol{U}=(U,\,W)$ and $\mathscr{U}=(\mathscr{U},\,\mathscr{W})$ denote the dimensionless velocity vectors of the water and mud skeleton in the x direction and z direction, respectively, μ represents the characteristic dynamic viscosity of the mud, $\tilde{\boldsymbol{\tau}}_{ij}$ and $\boldsymbol{\tau}_{ij}$ are the viscous stresses of the pore fluid and the viscoelastic stresses of the soil skeleton, respectively, $\tilde{\boldsymbol{\varepsilon}}_{ij}$ and $\boldsymbol{\varepsilon}_{ij}$ denote the strain tensors of the pore fluid and soil skeleton, respectively, and

$$\epsilon=\frac{\omega^2 A}{g} \tag{2.3}$$

measures the wave slope, which is typically small. In this study, the superscript prime indicates that the variable is dimensional and the tension is considered positive for the analysis.

https://doi.org/10.1017/jfm.2026.11447 Published online by Cambridge University Press

2.1. *Governing equations for the wave motion and mud dynamics*

For coastal water waves, the phase speed is significantly lower than that of the compressional wave in the water column (Abdolali *et al.* 2015). Thus, it is assumed that the upper layer of the water is incompressible. Employing (2.1), the dimensionless Navier–Stokes equations for wave motion can be written as (Wen & Liu 1995*b*)

$$\frac{\partial u}{\partial x}+\frac{\partial w}{\partial z}=0, \tag{2.4}$$

$$\frac{\partial u}{\partial t}+\epsilon\left(u\frac{\partial u}{\partial x}+w\frac{\partial u}{\partial z}\right)=-\frac{\partial p}{\partial x}+\frac{\delta_w^2}{2}\left(\frac{\partial^2 u}{\partial x^2}+\frac{\partial^2 u}{\partial z^2}\right), \tag{2.5}$$

$$\frac{\partial w}{\partial t}+\epsilon\left(u\frac{\partial w}{\partial x}+w\frac{\partial w}{\partial z}\right)=-\frac{\partial p}{\partial z}+\frac{\delta_w^2}{2}\left(\frac{\partial^2 w}{\partial x^2}+\frac{\partial^2 w}{\partial z^2}\right), \tag{2.6}$$

where δ_w is the normalised thickness of the bottom boundary layer of the water column, i.e.

$$\delta_w=\frac{\omega^2}{g}\sqrt{\frac{2\mu_w}{\rho\omega}}, \tag{2.7}$$

with μ_w denoting the dynamic viscosity of water. For water waves in the coastal region, δ_w is also a small parameter (Liu & Chan 2007*a*). Therefore, the flow in the water is essentially irrotational except in the boundary layer adjacent to the free surface and the bottom of the water column. In the core region of the water column, the governing equation of wave motion can be written as (Mei *et al.* 2010)

$$\frac{\partial^2 \Phi}{\partial x^2}+\frac{\partial^2 \Phi}{\partial z^2}=0. \tag{2.8}$$

The dynamic water pressure is related to the Bernoulli equation:

$$p+\frac{\partial \Phi}{\partial t}+\frac{\epsilon}{2}\left[\left(\frac{\partial \Phi}{\partial x}\right)^2+\left(\frac{\partial \Phi}{\partial z}\right)^2\right]=0. \tag{2.9}$$

Previous studies on wave propagation over muddy seabeds have predominantly employed single-phase medium models to characterise the dynamic response of the seabed (Dalrymple & Liu 1978; Macpherson 1980; Ng 2000; Ng & Zhang 2007; Mei *et al.* 2010; Garnier *et al.* 2013). However, such models inherently neglect the dynamic coupling between the pore fluid and mud skeleton (Yamamoto *et al.* 1978; Sumer 2014*b*). To address this knowledge gap, this study adopts the general two-phase poro-viscoelastic theory to formulate the governing equations for seabed soil motion. Within the muddy seabed, the continuity equation can be expressed as (Tong & Liu 2022)

$$n\frac{\partial}{\partial x}(U-\mathscr{U})+n\frac{\partial}{\partial Z}(W-\mathscr{W})+\frac{\partial \mathscr{U}}{\partial x}+\frac{\partial \mathscr{W}}{\partial Z}=-nM_a^2\frac{\partial P}{\partial t}, \tag{2.10}$$

in which M_a represents the Mach number, being defined as the ratio of the characteristic phase velocity of the water wave to the velocity of the compressible wave through the pore fluid,

$$M_a=\sqrt{\frac{\rho}{K}}\frac{g}{\omega}, \tag{2.11}$$

https://doi.org/10.1017/jfm.2026.11447 Published online by Cambridge University Press

with K indicating the apparent bulk modulus of elasticity of the pore fluid. As suggested by Verruit (1969), K depends on the degree of saturation S_r and is given by

$$\frac{1}{K} = \frac{1}{K_w} + \frac{1 - S_r}{p'_a}, \tag{2.12}$$

where K_w is the bulk modulus of elasticity of pure water and p'_a indicates the absolute pore water pressure. For analysis herein, $K_w = 2.3 \times 10^9$ Pa is used (Liu *et al.* 2007). Equation (2.10) shows that the motions of the pore fluid and the mud skeleton are affected by the compressibility of the pore fluid with the magnitude of this influence determined by the value of M_a. For an incompressible muddy seabed, $M_a = 0$.

The dimensionless momentum equations for the pore fluid are given by (Ouriemi, Aussilious & Guazzelli 2009; Baumgarten & Kamrin 2019*b*)

$$n\left(\frac{\partial U}{\partial t} + \epsilon \boldsymbol{U}\cdot\boldsymbol{\nabla} U\right) = -n\frac{\partial P}{\partial x} + \frac{1}{Re}\frac{A}{d}\left(\epsilon\frac{d}{A}\frac{\partial \tilde{\tau}_{xx}}{\partial x} + \frac{\partial \tilde{\tau}_{zx}}{\partial Z}\right) - \frac{n^2}{D_a}(U - \mathscr{U}), \tag{2.13}$$

$$n\left(\epsilon\frac{d}{A}\right)^2\left(\frac{\partial W}{\partial t} + \epsilon \boldsymbol{U}\cdot\boldsymbol{\nabla} W\right) = -n\frac{\partial P}{\partial Z} + \frac{\epsilon}{Re}\left(\epsilon\frac{d}{A}\frac{\partial \tilde{\tau}_{xz}}{\partial x} + \frac{\partial \tilde{\tau}_{zz}}{\partial Z}\right) - \left(\epsilon\frac{d}{A}\right)^2\frac{n^2}{D_a}(W - \mathscr{W}), \tag{2.14}$$

in which D_a is the Darcy number, which characterises the magnitude of the drainage flow within the muddy seabed and is defined as

$$D_a = \frac{\rho k_s \omega}{\mu_\omega}. \tag{2.15}$$

The dimensionless momentum equations for the skeleton frame of the mud read (Mei & Foda 1981; Baumgarten & Kamrin 2019*b*)

$$(1-n)\gamma\left(\frac{\partial \mathscr{U}}{\partial t} + \epsilon \mathscr{U}\cdot\boldsymbol{\nabla}\mathscr{U}\right) = -(1-n)\frac{\partial P}{\partial x} + \frac{1}{Re}\frac{A}{d}\left(\epsilon\frac{d}{A}\frac{\partial \tau_{xx}}{\partial x} + \frac{\partial \tau_{zx}}{\partial Z}\right) + \frac{n^2}{D_a}(U - \mathscr{U}), \tag{2.16}$$

$$(1-n)\gamma\left(\epsilon\frac{d}{A}\right)^2\left(\frac{\partial \mathscr{W}}{\partial t} + \epsilon \mathscr{U}\cdot\boldsymbol{\nabla}\mathscr{W}\right) = -(1-n)\frac{\partial P}{\partial Z} + \frac{\epsilon}{Re}\left(\epsilon\frac{d}{A}\frac{\partial \tau_{xz}}{\partial x} + \frac{\partial \tau_{zz}}{\partial Z}\right) + \frac{n^2}{D_a}\left(\epsilon\frac{d}{A}\right)^2(W - \mathscr{W}), \tag{2.17}$$

where γ is the density ratio of the mud particles ϱ to that of water ρ, and Re, called the Reynolds number, is the ratio between the viscous force and the elastic force, that is,

$$Re = \frac{\rho A \omega d}{\mu} \quad \text{and} \quad \mu = \sqrt{\mu_m^2 + \left(\frac{G}{\omega}\right)^2}, \tag{2.18}$$

where μ_m denotes the dynamic viscosity of mud due to grain-to-grain friction (Baumgarten & Kamrin 2019*a*; Zarch *et al.* 2025).

According to Newton's constitutive law and Hooke's law for compressible media, the viscoelastic stresses for the mud skeleton under simple harmonic wave loading can be

https://doi.org/10.1017/jfm.2026.11447 Published online by Cambridge University Press

expressed as (Macpherson 1980; Batchelor 2000)

$$\boldsymbol{\tau}_{ij} = \widetilde{\mu}\boldsymbol{\varepsilon}_{ij} + \widehat{\mu}\delta_{ij}\boldsymbol{\nabla}\cdot\mathscr{U}, \tag{2.19}$$

where $\boldsymbol{\nabla}$ denotes the gradient operator, i.e. $\boldsymbol{\nabla} = ((\partial/\partial x), (\partial/\partial Z))$, δ_{ij} indicates the Kronecker symbol, $\widetilde{\mu}$ and $\widehat{\mu}$ are complex constants, defined as

$$\widetilde{\mu} = \frac{\mu_m}{\mu} + \frac{\mathrm{i}G}{\mu\omega} = \mathrm{e}^{i\theta}, \qquad \widehat{\mu} = \mathrm{i}\frac{2\nu}{1-2\nu}\frac{G}{\mu\omega} - \frac{2\mu_m}{3\mu} \quad \text{and} \quad \theta = \arctan\left(\frac{G}{\mu_m\omega}\right), \tag{2.20}$$

with ν and i denoting Poisson's ratio and the imaginary unit, respectively. The mud viscosity μ_m represents the Coulomb damping due to the friction between grains (Yamamoto, Takahashi & Schuckman 1983) and θ is the argument of μ, which measures the relative importance of elasticity and viscosity, and it varies from 0 to $\pi/2$. For viscous-dominated mud, $\theta \to 0$ and for elastic-dominated mud, $\theta \to \pi/2$. The constitutive law, (2.19), is consistent with that developed by Si, Shi & Yu (2019).

Finally, the dimensionless strain tensor can be expressed as

$$\boldsymbol{\varepsilon}_{ij} = \begin{pmatrix} \varepsilon_{xx} & \varepsilon_{zx} \\ \varepsilon_{xz} & \varepsilon_{zz} \end{pmatrix} = \begin{pmatrix} 2\epsilon\dfrac{d}{A}\dfrac{\partial\mathscr{U}}{\partial x} & \dfrac{\partial\mathscr{U}}{\partial Z} + \left(\epsilon\dfrac{d}{A}\right)^2\dfrac{\partial\mathscr{W}}{\partial x} \\ \dfrac{\partial\mathscr{U}}{\partial Z} + \left(\epsilon\dfrac{d}{A}\right)^2\dfrac{\partial\mathscr{W}}{\partial x} & 2\epsilon\dfrac{d}{A}\dfrac{\partial\mathscr{W}}{\partial Z} \end{pmatrix}. \tag{2.21}$$

For incompressible mud, $\boldsymbol{\nabla}\cdot\mathscr{U} = 0$, and then the constitutive law, (2.19), reduces to the Kelvin-Voigt model used in Macpherson (1980) and Garnier *et al.* (2013).

2.2. *Boundary conditions*

The free surface is a material surface, thus, the kinematic condition is given by

$$\frac{\partial\eta}{\partial t} = \frac{\partial\Phi}{\partial z} - \epsilon\frac{\partial\eta}{\partial x}\frac{\partial\Phi}{\partial x}, \qquad z = \epsilon\eta. \tag{2.22}$$

Assuming that the atmospheric pressure is uniform zero at the free surface, for the potential flow, the dynamic boundary condition at the free surface can be written as

$$\eta + \frac{\partial\Phi}{\partial t} + \frac{\epsilon}{2}\left[\left(\frac{\partial\Phi}{\partial x}\right)^2 + \left(\frac{\partial\Phi}{\partial z}\right)^2\right] = 0, \qquad z = \epsilon\eta. \tag{2.23}$$

The two conditions, (2.22) and (2.23), can be combined into one in terms of Φ, taking the total derivative of (2.23):

$$\left(\frac{\partial}{\partial Z} + \frac{\partial^2}{\partial t^2}\right)\Phi + \epsilon\left[\frac{\partial}{\partial t} + \frac{\epsilon}{2}\left(\frac{\partial\Phi}{\partial x}\frac{\partial}{\partial x} + \frac{\partial\Phi}{\partial z}\frac{\partial}{\partial z}\right)\right]\left[\left(\frac{\partial\Phi}{\partial x}\right)^2 + \left(\frac{\partial\Phi}{\partial z}\right)^2\right] = 0, \quad z = \epsilon\eta. \tag{2.24}$$

At the water–seabed interface, the kinematic condition is given by

$$\frac{d}{A}\mathscr{W} = \frac{\partial\zeta}{\partial t} + \epsilon\mathscr{U}\frac{\partial\zeta}{\partial x}, \qquad Z = 1 + \epsilon\frac{A}{d}\zeta \tag{2.25}$$

for the muddy seabed, and

$$\frac{\partial\Phi}{\partial z} = \epsilon\frac{\partial\zeta}{\partial t} + \epsilon^2\frac{\partial\Phi}{\partial x}\frac{\partial\zeta}{\partial x}, \qquad z = -h + \epsilon^2\zeta \tag{2.26}$$

https://doi.org/10.1017/jfm.2026.11447 Published online by Cambridge University Press

for water, where h is the normalised depth of the water column. The velocity of the pore fluid and water must be continuous,

$$u = U, \qquad w = \frac{d}{A}\epsilon W, \qquad z = -h + \epsilon^2\zeta. \tag{2.27}$$

Since the mud seabed is porous, the pressure will also be continuous at the water–seabed interface, i.e.

$$p = P, \qquad z = -h + \epsilon^2\zeta. \tag{2.28}$$

Meanwhile, continuity of the stresses at the water–mud interface requires that

$$\tilde{\tau}_{xx}n_x + \tilde{\tau}_{zx}n_z = 2\epsilon\frac{d}{A}\frac{\partial u}{\partial x}n_x + \epsilon\frac{d}{A}\left(\frac{\partial w}{\partial x} + \frac{\partial u}{\partial z}\right)n_z, \qquad z = -h + \epsilon^2\zeta, \tag{2.29}$$

$$\tilde{\tau}_{xz}n_x + \tilde{\tau}_{zz}n_z = \epsilon\frac{d}{A}\left(\frac{\partial w}{\partial x} + \frac{\partial u}{\partial z}\right)n_x + 2\epsilon\frac{d}{A}\frac{\partial w}{\partial z}n_z, \qquad z = -h + \epsilon^2\zeta \tag{2.30}$$

for water, and

$$(\tau_{x0} + \tau_{xx})n_x + \tau_{zx}n_z = 0, \qquad Z = 1 + \epsilon\frac{A}{d}\zeta, \tag{2.31}$$

$$\tau_{xz}n_x + (\tau_{z0} + \tau_{zz})n_z = 0, \qquad Z = 1 + \epsilon\frac{A}{d}\zeta \tag{2.32}$$

for the soil skeleton, where n_x and n_z are the horizontal and vertical components of the unit normal vector of the water–mud interface:

$$n_x = \frac{\epsilon^2\dfrac{d}{A}\dfrac{\partial\zeta}{\partial x}}{\sqrt{1 + \left(\epsilon^2\dfrac{d}{A}\dfrac{\partial\zeta}{\partial x}\right)^2}}, \qquad n_z = \frac{1}{\sqrt{1 + \left(\epsilon^2\dfrac{d}{A}\dfrac{\partial\zeta}{\partial x}\right)^2}}. \tag{2.33}$$

Clearly, n_x and n_z are of the order of magnitude of $O(\epsilon^2)$ and $O(1)$, respectively. In (2.31) and (2.32), τ_{x0} and τ_{z0} are normal stresses in the hydrostatic state in the x and z directions, respectively. Under the hydrostatic equilibrium condition, the shear stress of the mud skeleton vanishes, and the normal effective stresses are given by (Madsen 1978; Tong & Liu 2022)

$$\tau_{x0} = \frac{\nu}{1-\nu}\frac{d}{A}\gamma_e(Z-1), \qquad \tau_{z0} = \frac{d}{A}\gamma_e(Z-1), \tag{2.34}$$

where $\gamma_e = (1-n)(\gamma - 1)$ is the ratio of the submerged unit weight of mud to the unit weight of water.

Following Tong & Liu (2022), the bottom of the seabed is assumed to be rigid and impermeable. The horizontal and vertical velocity components of the mud skeleton are equal to zero, and the vertical pressure gradient vanishes:

$$\mathscr{U} = \mathscr{W} = \frac{\partial P}{\partial Z} = 0, \qquad Z = 0. \tag{2.35}$$

The boundary conditions indicate that the mud is forced to move passively by the hydrodynamic pressure and the viscous stresses from the surface waves. To solve this coupled boundary value problem, we introduce simplifying assumptions grounded in the characteristic scales of coastal waves and the rheological properties of mud. Subsequently, we apply a multiscale perturbation method to obtain analytical solutions for the flow fields

https://doi.org/10.1017/jfm.2026.11447 Published online by Cambridge University Press

in both the water column and the muddy seabed. The key assumptions and the solution procedure are detailed in the following subsections.

3. Scalings and assumptions

In this study we focus on investigating the wave propagating over a thin mud layer. Therefore, following Liu & Chan (2007*b*), the thickness of the muddy seabed is assumed to be of the same order of magnitude as the wave amplitude, i.e.

$$O\left(\frac{d}{A}\right) \sim O(1). \tag{3.1}$$

The apparent bulk modulus of elasticity of the pore fluid, K, is sensitive to S_r (Liu *et al.* 2007). For example, when S_r decreases from 1 to 0.9, K decreases from 2.3×10^9 Pa to 1×10^6 Pa for the mud under a water depth of 10 m. Correspondingly, the velocity of the compressible wave within the pore fluid is close to the phase velocity of the wind waves. Therefore, the Mach number is treated as being of the order of magnitude of $O(1)$:

$$O\left(M_a\right) \sim O(1). \tag{3.2}$$

This assumption agrees well with some *in situ* measurements. For example, Bennett & Faris (1979) reports that the saturation degree of the mud in the Mississippi Delta is 0.9, and therefore, $M_a = 0.63$ when $h = 10$ m and $\omega = 0.5\ \mathrm{s}^{-1}$, and $M_a = 1.05$ when $h = 10$ m and $\omega = 0.3\ \mathrm{s}^{-1}$. For a highly saturated seabed, $M_a \to 0$, and further simplification is possible.

The shear modulus ranges widely from $O(10^3\ \mathrm{Pa})$ for soft seabeds to $O(10^8\ \mathrm{Pa})$ for dense seabeds (Yamamoto *et al.* 1978; Macpherson 1980; Liu & Chan 2007*b*), and the mud viscosity varies from $O(10\ \mathrm{Pa\,s})$ to $O(10^4\ \mathrm{Pa\,s})$. Correspondingly, the Reynolds number, Re, varies from $O(10^{-5})$ to $O(10)$ (Wen & Liu 1995*a*). For a stiff seabed, Re is small, indicating that the inertia force is less important. For a soft muddy seabed, Re is relatively large. For example, the characteristic mud viscosity in Lianyungang, China is of the order of magnitude of $O(10^3\ \mathrm{Pa\,s}) - O(10^4\ \mathrm{Pa\,s})$ when $n = 0.5$ (Mei *et al.* 2010; Garnier *et al.* 2013). As a rough estimation, $Re = 1.0$ when $\mu = 10^3$ Pa s, and $Re = 0.1$ when $\mu = 10^4$ Pa s together with $\omega = 1.0\ \mathrm{rad\,s}^{-1}$ and $A = d = 1.0$ m. Therefore, Re is also assumed to be of the order of magnitude of $O(1)$, that is,

$$O(Re) \sim O(M_a) \sim O(1). \tag{3.3}$$

Physically, it means that viscous and elastic effects throughout the mud seabed are treated without the boundary layer approximation.

For the muddy seabed, the Darcy number, D_a, is very small. For example, k_s is of the order of magnitude of $O(10^{-13}\ \mathrm{m}^2)$ or even smaller in a silty or clayey seabed (Liu *et al.* 2007). For approximation, we take $k_s = 10^{-13}\ \mathrm{m}^2$, $\omega = 0.5\ \mathrm{rad\,s}^{-1}$ and $\mu_w = 10^{-3}$ Pa s, then $D_a = 5 \times 10^{-8}$. Therefore, the following relation with respect to D_a and ϵ shall be satisfied:

$$O(D_a) \ll O(\epsilon^3) \ll O(\epsilon) \ll 1. \tag{3.4}$$

This means that the drainage effects are negligible for the wave-induced mud dynamics.

For waves in the coastal region, the thickness of the bottom boundary layer is usually small and is assumed to be $O(\epsilon)$ (Longguet-Higgins 1953; Ng 2000), that is,

$$O(\delta_w) \sim O(\epsilon) \ll 1. \tag{3.5}$$

https://doi.org/10.1017/jfm.2026.11447 Published online by Cambridge University Press

In estimation, take $\omega = 0.5$–$2\ \mathrm{rad\,s^{-1}}$ and eddy viscosity $\mu_w = 1.0\ \mathrm{Pa\,s}$, then $\delta_w = 0.16$–1.3×10^{-2}. Thus, the above assumption is approximately satisfied.

4. Perturbation analysis

Based on (3.1)–(3.5), the dynamics of the flow problem can be presented in the following manner. In the core region of the water column, the flow is irrotational and can be described by potential flow theory. Given that the vertical displacement of the water–seabed interface is small, $O(\epsilon)$, and the drainage flow is quite weak, $O(D_a)$, in the leading-order problem, the wave motion does not sense the muddy seabed and so the solution for irrotational motion coincides with the well-known potential flow solution for small-amplitude waves over a solid bottom. However, the dynamic pressure at the water–seabed interface induces a shear flow within the muddy seabed. The horizontal and vertical velocity components of the shear flow are of the order of magnitude of $O(1)$ and $O(\epsilon)$, respectively. Meanwhile, a leading-order horizontal rotational velocity develops within the bottom boundary layer of the water column to satisfy the continuity of velocity and viscous shear stress across the interface. According to the continuity equation, a vertical velocity component of $O(\delta_w)$ must also arise within this boundary layer. As a result, the irrotational flow in the core region must be corrected at $O(\delta_w)$. Due to the nonlinear interactions between the velocity components, mass transport occurs within the water column and muddy seabed, which is of the order of magnitude of $O(\epsilon)$. The rotational horizontal velocity within the free surface boundary layer, $O(\delta_w)$, is weaker since only the zero shear stress is imposed at the free surface (Mei & Liu 1973), and correspondingly, the vertical rotational velocity inside this boundary layer is $O(\delta_w^2)$, which has no influence on wave and mud motions, correct to $O(\epsilon)$, except for introducing a second-order mean Eulerian vorticity outside the boundary layer.

In the dimensionless governing equations and boundary conditions, ϵ, D_a and δ_w are three small dimensionless parameters. For small-amplitude progressive waves, it is natural to employ the asymptotic method of perturbations. According to (3.1)−(3.5), ϵ is chosen as the ordering small parameter. Anticipating that wave damping will become significant only after propagating over a long distance, the following multiple-scale coordinates are introduced in terms of ϵ,

$$t, \quad t_1 = \epsilon t, \quad t_2 = \epsilon^2 t, \cdots; \qquad x, \quad x_1 = \epsilon x, \quad x_2 = \epsilon^2 x, \cdots. \tag{4.1}$$

The derivatives with respect to t must now be replaced by

$$\frac{\partial}{\partial t} = \frac{\partial}{\partial t} + \epsilon \frac{\partial}{\partial t_1} + \epsilon^2 \frac{\partial}{\partial t_2} + \cdots, \quad \frac{\partial^2}{\partial t^2} = \frac{\partial^2}{\partial t^2} + 2\epsilon \frac{\partial^2}{\partial t \partial t_1} + \epsilon^2 \left(\frac{\partial^2}{\partial t_1^2} + \frac{\partial^2}{\partial t \partial t_2} \right) + \cdots. \tag{4.2}$$

Similar replacements must be made for derivatives with respect to x, while derivatives with respect to z and Z remain the same.

For slowly varying harmonic waves, the variables, such as Φ, p, P, (u, w), (U, W) and τ_{ij}, can be expanded as follows:

$$\mathscr{F} = \frac{1}{2}\left[\mathscr{F}_0 + \epsilon \mathscr{F}_1 + \epsilon^2 \mathscr{F}_2 + \cdots\right] \mathrm{e}^{\mathrm{i}(kx - t)} + \text{c.c.} \tag{4.3}$$

Here (η_n, ζ_n) depend only on $(x_1, \cdots; t_1, \cdots)$, Φ_n on $(x_1, \cdots; z; t_1, \cdots)$ in the water column and (U_n, W_n, u_n, w_n) on $(x_1, \cdots; Z; t_1, \cdots)$ in the muddy seabed, 'c.c.' denotes the conjugate complex of the preceding terms. In addition, there is an additional horizontal

https://doi.org/10.1017/jfm.2026.11447 Published online by Cambridge University Press

length scale due to the motion of the muddy seabed, $O(1/k\epsilon)$, and therefore, the wavenumber is also expanded in power of ϵ:

$$k = k_0 + \epsilon k_1 + \epsilon^2 k_2 + \cdots. \tag{4.4}$$

Since the free surface oscillates with displacement of $\epsilon\eta$, the general variable, $\mathscr{F}$, can be expanded in terms of the Taylor series, i.e.

$$\mathscr{F}(x, \epsilon\eta, t) = \mathscr{F}(x, 0, t) + \epsilon\eta \left.\frac{\partial \mathscr{F}}{\partial z}\right|_{z=0} + \epsilon^2\eta^2 \frac{1}{2} \left.\frac{\partial^2 \mathscr{F}}{\partial z^2}\right|_{z=0} + \cdots. \tag{4.5}$$

Similarly, at the water–mud interface, $\mathscr{F}$ can be expanded as

$$\mathscr{F}(x, -h + \epsilon^2\zeta, t) = \mathscr{F}(x, -h, t) + \epsilon^2\zeta \left.\frac{\partial \mathscr{F}}{\partial z}\right|_{z=-h} + \cdots \tag{4.6}$$

for the variables within the water column, and

$$\mathscr{F}(x, 1 + \epsilon\frac{A}{d}\zeta, t) = \mathscr{F}(x, 1, t) + \epsilon\frac{A}{d}\zeta \left.\frac{\partial \mathscr{F}}{\partial Z}\right|_{Z=1} + \frac{1}{2}\left(\epsilon\frac{A}{d}\zeta\right)^2 \left.\frac{\partial \mathscr{F}}{\partial Z}\right|_{Z=1} + \cdots \tag{4.7}$$

for the variables within the muddy seabed.

Substituting the expansions (4.1)–(4.6) into the dimensionless governing equations and boundary conditions, a series of perturbation equations can be obtained after separating the orders. In this study the leading-order and second-order boundary value problems are solved and investigated in detail.

5. Leading-order boundary value problems for water and mud motions

Based on the assumptions given in § 3, the leading-order boundary value problems for water and mud motions are summarised and solved in this section, respectively.

5.1. *Inviscid flow within the water column*

At the leading order, the oscillation of the water–seabed interface and the nonlinear terms have no influence on the wave motion. Correspondingly, the boundary value problem for the wave motion can be summarised as

$$-k_0^2\Phi_0 + \frac{d^2\Phi_0}{\mathrm{d}z^2} = 0, \quad -h < z < 0, \tag{5.1}$$

with

$$\frac{\partial \Phi_0}{\partial z} - \Phi_0 = 0, \quad z = 0, \tag{5.2}$$

$$\frac{\partial \Phi_0}{\partial z} = 0, \quad z = 0. \tag{5.3}$$

$$\eta_0 = \mathrm{i}\Phi_0, \quad z = 0. \tag{5.4}$$

The leading-order solution for the velocity potential Φ_0 can be readily obtained by solving the two-point boundary value problem (5.1)–(5.3), which can be written as

$$\Phi_0 = -\mathrm{i}\hat{A}\frac{\cosh Q}{\cosh q}, \tag{5.5}$$

where

$$Q \equiv k_0(z + h), \quad q \equiv k_0 h. \tag{5.6}$$

https://doi.org/10.1017/jfm.2026.11447 Published online by Cambridge University Press

Based on (5.4), the free surface elevation can be written as

$$\eta_0 = \hat{A}, \tag{5.7}$$

with the dispersion relationship of

$$k_0 \tanh k_0 h = 1. \tag{5.8}$$

It should be remarked that $\hat{A}$ depends on the slow coordinates and is yet unknown. For later use, the potential velocity components of water are calculated by differentiating the velocity potential with respect to x and z, respectively, that is,

$$\widehat{u}_0 = \frac{\partial \Phi_0}{\partial x} = k_0 \hat{A} \frac{\cosh Q}{\cosh q} = \hat{A} \frac{\cosh Q}{\sinh q}, \tag{5.9}$$

$$\widehat{w}_0 = \frac{\partial \Phi_0}{\partial z} = -\mathrm{i} k_0 \hat{A} \frac{\sinh Q}{\cosh q} = -\mathrm{i} \hat{A} \frac{\sinh Q}{\sinh q}. \tag{5.10}$$

According to (2.9), the following leading-order dynamic pressure can be obtained:

$$p_0 = \mathrm{i}\Phi_0 = \hat{A} \frac{\cosh Q}{\cosh q}. \tag{5.11}$$

This has a finite value along the water bottom, $z = -h$,

$$p_b = p_0|_{z=-h} = \frac{\hat{A}}{\cosh q}, \tag{5.12}$$

and, in turn, it generates muddy flow within the seabed.

5.2. *Viscid flows within the Stokes boundary layer and muddy seabed*

Since the Stokes boundary layer in water is thin, a stretched coordinate ξ is introduced as

$$\xi = \frac{z + h}{\delta_w}. \tag{5.13}$$

Hence, the continuity equation for the rotational velocity components can be written as

$$\mathrm{i} k_0 u_0^r + \frac{1}{\delta_w} \frac{\partial w_0^r}{\partial \xi} = 0, \qquad 0 < \xi < \infty. \tag{5.14}$$

According to (2.5), the governing equation of the rotational component of the horizontal velocity can be expressed as

$$\frac{\partial^2 u_0^r}{\partial \xi^2} + 2\mathrm{i} u_0^r = 0, \qquad 0 < \xi < \infty. \tag{5.15}$$

Based on (2.13), (2.14), (3.4) and (3.5), it is known that

$$U_0 = \mathscr{U}_0, \qquad 0 < Z < 1, \tag{5.16}$$

$$W_0 = \mathscr{W}_0, \qquad 0 < Z < 1, \tag{5.17}$$

correct to $O(Da)$, indicating that the pore fluid moves with the mud skeleton as a block in the leading-order boundary value problem. Therefore, the continuity equation of the muddy flow can be written as

$$\mathrm{i} k_0 \mathscr{U}_0 + \frac{\partial \mathscr{W}_0}{\partial Z} = \mathrm{i} n M_a^2 P_0, \qquad 0 < Z < 1. \tag{5.18}$$

Since the pore fluid moves with the mud skeleton as a block, the viscosity of the pore fluid can be absorbed into that of the mud skeleton. Thus, hereinafter μ_m stands for the total

https://doi.org/10.1017/jfm.2026.11447 Published online by Cambridge University Press

viscosity of the mud block. Combining the momentum equations for the mud skeleton with that for the pore fluid, the leading-order momentum equations for the mud block are obtained to be

$$-\mathrm{i}\gamma_m \mathscr{U}_0 = -\mathrm{i}k_0 P_0 + \frac{\widetilde{\mu}}{Re}\frac{A}{d}\frac{d^2\mathscr{U}_0}{\mathrm{d}Z^2}, \qquad 0 < Z < 1, \tag{5.19}$$

$$\frac{\partial P_0}{\partial Z} = 0, \qquad 0 < Z < 1, \tag{5.20}$$

where γ_m is the density ratio of the mud block to water, namely $\gamma_m = (1-n)\gamma + n$. Based on (5.20), it is known that the dynamic pore pressure is uniform in the Z direction,

$$P_0 = p_b = \frac{\hat{A}}{\cosh q}. \tag{5.21}$$

Thus, the boundary value problem for the horizontal velocity of the mud can be expressed as

$$\frac{d^2\mathscr{U}_0}{\mathrm{d}Z^2} - \sigma^2\mathscr{U}_0 = -\frac{\sigma^2}{\gamma_m}\frac{\hat{A}}{\sinh q}, \qquad 0 < Z < 1, \tag{5.22}$$

where

$$\sigma = \sqrt{-\mathrm{i}\gamma_m \frac{Re}{\widetilde{\mu}}\frac{d}{A}} = \sqrt{2}\widehat{d}\,\mathrm{e}^{-\mathrm{i}\left(\frac{\theta}{2}+\frac{\pi}{4}\right)}, \quad \widehat{d} = \frac{d}{\delta'_m} \text{ and } \delta'_m = \sqrt{\frac{2\mu}{\rho_m\omega}}, \tag{5.23}$$

with ρ_m and δ'_m denoting the density of the mud and the thickness of the Stokes boundary layer of the muddy seabed, respectively.

Since the flow in the core region is inviscid, the rotational velocity vanishes beyond the Stokes boundary layer ($\xi \to \infty$). At the water–seabed interface, the velocity and shear stress are continuous. At the bottom of the seabed, the horizontal velocity component is equal to zero. Therefore, the following conditions are satisfied for viscid flows within the Stokes boundary layer and muddy seabed:

$$\frac{\partial u_0^r}{\partial \xi} = 0, \qquad \xi \to \infty, \tag{5.24}$$

$$\mathscr{U}_0 = \frac{\hat{A}}{\sinh q} + u_0^r, \qquad \xi = 0 \text{ (or } Z = 1), \tag{5.25}$$

$$\mu\mathrm{e}^{\mathrm{i}\theta}\frac{\partial \mathscr{U}_0}{\partial Z} = \epsilon\frac{d}{A}\frac{\mu_w}{\delta_w}\frac{\partial u_0^r}{\partial \xi}, \qquad \xi = 0 \text{ (or } Z = 1), \tag{5.26}$$

$$\mathscr{U}_0 = 0, \qquad Z = 0. \tag{5.27}$$

The boundary value problem (5.15), (5.22) and (5.24)–(5.27) can be explicitly solved, and the solution can be written as

$$u_0^r = D\frac{\hat{A}}{\sinh q}\mathrm{e}^{-(1-\mathrm{i})\xi}, \tag{5.28}$$

$$\mathscr{U}_0 = \frac{1}{\gamma_m}\frac{\hat{A}}{\sinh q}\left(1 - \cosh(\sigma Z) + F\sinh(\sigma Z)\right), \tag{5.29}$$

where

$$D = \frac{-\beta - \beta(\gamma_m - 1)\cosh\sigma}{\gamma_m\beta\cosh\sigma + \sinh\sigma}, \tag{5.30}$$

https://doi.org/10.1017/jfm.2026.11447 Published online by Cambridge University Press

$$F = \frac{\gamma_m - 1 + \cosh\sigma + \beta\gamma_m \sinh\sigma}{\gamma_m \beta \cosh\sigma + \sinh\sigma}. \tag{5.31}$$

In (5.30) and (5.31), $\beta = \delta_m' \mathrm{e}^{\mathrm{i}(\theta/2)}/\delta_w'$ measures the ratio of the Stokes boundary layer thickness. Since mud is typically more viscous than water, β is commonly much larger than unity (Liu & Chan 2007*a*; Garnier *et al.* 2013). If mud is pure viscous, the solution of u_0^r and $\mathscr{U}_0$, (5.28) and (5.29), agrees with the results of Ng (2000), and if the viscosity of water is ignored, $\beta \to \infty$, then (5.29) reduces to the results of Mei *et al.* (2010).

At the bottom of the seabed, the leading-order vertical velocity component of mud vanishes. Thus, substituting (5.29) and (5.21) into (5.18) and integrating with respect to Z from 0 to Z yields the vertical velocity component of mud flow:

$$\mathscr{W}_0 = \mathrm{i}nM_a^2 \frac{\hat{A}}{\cosh q} Z - \mathrm{i}\frac{k_0}{\gamma_m}\frac{\hat{A}}{\sinh q}\left[Z - \frac{\sinh(\sigma Z)}{\sigma} + F\frac{\cosh(\sigma Z) - 1}{\sigma}\right]. \tag{5.32}$$

The first term on the right-hand side of (5.32) signifies the effect of compressibility on mud motion. For an incompressible muddy seabed, $M_a = 0$ and $\mathscr{W}_0$ reduces to the result of Ng & Zhang (2007). Inside the bottom boundary layer, the total horizontal velocity component, u_0, can be written as

$$u_0 = \widehat{u}_0 + u_0^r = \left[1 + D\mathrm{e}^{-(1-\mathrm{i})\xi}\right]\frac{\hat{A}}{\sinh q}. \tag{5.33}$$

If $d = 0$ then $\sigma = 0$, therefore, $\cosh\sigma = 1$ and $\sinh\sigma = 0$. Consequently, $D = -1$ and (5.33) reduces to the results of Mei *et al.* (2005). At the water–seabed interface, the vertical velocity component of mud and water should also be continuous, and w_0 vanishes. Thus, based on (5.14), the vertical rotational velocity component can be found by integration with respect to ξ, i.e.

$$w_0^r = \epsilon\frac{d}{A}\left(\mathrm{i}nM_a^2\frac{\hat{A}}{\cosh q} - \mathrm{i}\frac{k_0}{\gamma_m}\frac{\hat{A}}{\sinh q}\mathscr{G}(\sigma,\beta)\right) + \mathrm{i}\delta_w D\frac{k_0\hat{A}}{\sinh q}\frac{\mathrm{e}^{-(1-\mathrm{i})\xi} - 1}{1-\mathrm{i}}, \tag{5.34}$$

where

$$\mathscr{G}(\sigma,\beta) = 1 - \frac{\sinh\sigma}{\sigma} + F\frac{\cosh\sigma - 1}{\sigma}. \tag{5.35}$$

Accordingly, the total vertical velocity component, w_0, within the bottom boundary layer is given by

$$w_0 = \epsilon\frac{d}{A}\mathscr{W}_s - \mathrm{i}\delta_w\frac{k_0\hat{A}}{\sinh q}\left[\xi - D\frac{\mathrm{e}^{-(1-\mathrm{i})\xi} - 1}{1-\mathrm{i}}\right], \tag{5.36}$$

where $\mathscr{W}_s$ is the vertical velocity component of the mud at the water–seabed interface, i.e.

$$\mathscr{W}_s = \mathrm{i}\frac{k_0\hat{A}}{\sinh q}\left(nM_a^2\tanh^2 q - \frac{\mathscr{G}(\sigma,\beta)}{\gamma_m}\right). \tag{5.37}$$

Equation (5.36) demonstrates that the vertical velocity component is of order $O(\epsilon)$, which is one order of magnitude smaller than the horizontal velocity component. Finally, the vertical displacement of the water–seabed interface, ζ_0, is calculated from (2.25) at the leading order:

$$\zeta_0 = \mathrm{i}\frac{d}{A}\mathscr{W}_s = \frac{d}{A}\frac{k_0\hat{A}}{\sinh q}\left(\frac{\mathscr{G}(\sigma,\beta)}{\gamma_m} - nM_a^2\tanh^2 q\right). \tag{5.38}$$

We reiterate that $\hat{A}$, which depends on the slow coordinates, is still unknown.

https://doi.org/10.1017/jfm.2026.11447 Published online by Cambridge University Press

The leading-order solutions above reveal that, although seabed compressibility exerts no influence on the leading-order horizontal velocity components in either the water column or the muddy seabed, it does induce measurable deviations in the vertical velocity component within both the Stokes boundary layer and the muddy seabed, relative to predictions from single-phase incompressible models. Crucially, this compressibility-induced deviation cannot be compensated by adjusting the shear modulus or viscosity of the mud in single-phase incompressible models.

6. The second-order boundary value problems

6.1. *Evolution of the wave envelope*

The governing equation of the first-order velocity potential can be expressed as

$$\frac{\partial^2 \Phi_1}{\partial z^2} - k_0^2 \Phi_1 = -2\mathrm{i}k_0 \frac{\partial \Phi_0}{\partial x_1} = -2k_0 \frac{\cosh Q}{\cosh q} \frac{\partial \hat{A}}{\partial x_1}, \tag{6.1}$$

and the boundary conditions are given by

$$\frac{\partial \Phi_1}{\partial z} - \Phi_1 = 2\mathrm{i}\frac{\partial \Phi_0}{\partial t_1} = 2\frac{\partial \hat{A}}{\partial t_1}, \qquad z = 0, \tag{6.2}$$

$$\frac{\partial \Phi_1}{\partial z} = -\mathrm{i}\zeta_0, \qquad z = -h. \tag{6.3}$$

The boundary value problem (6.1)–(6.3) is non-homogeneous. Since the homogeneous version of the boundary value problem has Φ_0 as a non-trivial solution, the non-homogeneous problem must satisfy a solvability condition, which follows by applying Green's theorem to Φ_0 and Φ_1 (Mei *et al.* 2005):

$$\int_{-h}^{0} \left[\Phi_0 \left(\frac{\partial^2 \Phi_1}{\partial z^2} - k_0^2 \Phi_1 \right) + \Phi_1 \left(\frac{\partial^2 \Phi_0}{\partial z^2} - k_0^2 \Phi_0 \right) \right] \mathrm{d}z = \left(\Phi_0 \frac{\partial \Phi_1}{\partial z} - \Phi_1 \frac{\partial \Phi_0}{\partial z} \right) \Big|_{z=-h}^{z=0}. \tag{6.4}$$

Substituting (5.1)–(5.3) and (6.1)–(6.3) into (6.4) yields the following evolution equation of the free surface elevation $\hat{A}$:

$$\frac{\partial \hat{A}}{\partial t_1} + C_g \frac{\partial \hat{A}}{\partial x_1} = \mathrm{i}k_1 C_g \hat{A}. \tag{6.5}$$

Here C_g is the dimensionless wave group velocity,

$$C_g = \frac{1}{2k_0} \left(1 + \frac{2q}{\sinh 2q} \right), \tag{6.6}$$

and the first-order wavenumber k_1 is given by

$$k_1 = -\frac{1}{\gamma_m} \frac{d}{A} \frac{2k_0^2}{\sinh 2q + 2q} \left(\mathscr{G}(\sigma, \beta) - nM_a^2 \gamma_m \tanh^2 q \right). \tag{6.7}$$

The right-hand side of (6.5) signifies the effect of the mud motion on the evolution of the envelope of the leading-order wave. For simple harmonic waves, the wave envelope is independent of t_1, and therefore, the wave amplitude $\hat{A}$ can be found as

$$\hat{A} = A_0 \mathrm{e}^{\mathrm{i}k_1 x_1} = A_0 \mathrm{e}^{-\epsilon k_1^i x} \mathrm{e}^{\mathrm{i}\epsilon k_1^r x}, \qquad x_1 > 0, \tag{6.8}$$

where A_0 is the normalised wave amplitude at $x_1 = 0$ that can be taken to be unity, k_1^r and k_1^i are the real and imaginary parts of k_1, respectively. According to (6.8), it is known that

https://doi.org/10.1017/jfm.2026.11447 Published online by Cambridge University Press

due to the flow within the muddy seabed, the surface wave damps slowly at a rate of ϵk_1^i and with a phase shift of ϵk_1^r.

Substituting (6.8) into (6.1) and (6.2), now the boundary value problem (6.1)–(6.3) can be solved straightforwardly, and the solution can be written as

$$\Phi_1 = 2\mathrm{i}k_1 C_g \hat{A} \sinh q \sinh Q - \frac{1}{k_0}\frac{Q \sinh Q}{\cosh q}\frac{\partial \hat{A}}{\partial x_1}, \tag{6.9}$$

$$P_1 = -\left(\frac{\partial \Phi_0}{\partial t_1} + \frac{\partial \Phi_1}{\partial t}\right) = \frac{\mathrm{i}}{\cosh q}\left(\frac{\partial \hat{A}}{\partial t_1}\cosh Q - \frac{Q}{k_0}\frac{\partial \hat{A}}{\partial x_1}\sinh Q\right) - 2k_1 C_g \hat{A}\sinh q \sinh Q, \tag{6.10}$$

$$\eta_1 = -\left(\frac{\partial \Phi_0}{\partial t_1} + \frac{\partial \Phi_1}{\partial t}\right)\bigg|_{z=0} = \mathrm{i}\left(\frac{\partial \hat{A}}{\partial t_1} - \frac{q\tanh q}{k_0}\frac{\partial \hat{A}}{\partial x_1}\right) - 2k_1 C_g \hat{A}\sinh^2 q. \tag{6.11}$$

For highly saturated muddy seabeds, $M_a \to 0$ and (6.9)–(6.11) reduce to those of Mei *et al.* (2010).

6.2. *Wave-induced steady currents*

In the water column the boundary layer adjacent to the free surface is responsible for introducing a second-order mean vorticity, called mean Eulerian vorticity, outside this boundary layer (Longguet-Higgins 1953, 1960). This mean vorticity is given by (see Appendix A)

$$\frac{\partial \overline{u}_1}{\partial z} = 2\mathrm{i}\frac{\partial^2 \Phi_0}{\partial x^2}\frac{\partial^2 \Phi_0^*}{\partial x \partial z} = -2k_0^3|\hat{A}|^2, \qquad z = 0, \tag{6.12}$$

where the asterisk denotes the complex conjugate and the overbar indicates the time average over a wave period. Mathematically, for a general variable $\mathscr{F}$,

$$\overline{\mathscr{F}} = \frac{1}{T}\int_t^{t+T} \mathscr{F}\,\mathrm{d}t, \tag{6.13}$$

where $T = 2\pi/\omega$ is the wave period. Since the free surface is a material surface, the vertical component of the steady current $\overline{w}_1$ must vanish, i.e.

$$\overline{w}_1 = 0, \qquad z = 0. \tag{6.14}$$

Within the bottom boundary layer of the water column, the time-averaged equation of u_1 can be written as (Wen & Liu 1995*a*)

$$\frac{\partial^2 \overline{u}_1}{\partial \xi^2} = -(1-\mathrm{i})D\frac{\hat{A}}{\sinh q}\left(\frac{\epsilon}{\delta_w}\frac{d}{A}\mathscr{W}_s - \mathrm{i}\frac{k_0\hat{A}}{\sinh q}H(\xi)\right)^* \mathrm{e}^{-(1-\mathrm{i})\xi}, \tag{6.15}$$

and within the muddy seabed, that of $\mathscr{U}_1$ can be expressed as (Ng & Zhang 2007)

$$\frac{\partial^2 \overline{\mathscr{U}}_1}{\partial Z^2} = \frac{\mathrm{i}}{2}\frac{\sigma^3}{\gamma_m}\frac{\hat{A}}{\sinh q}\left[F\cosh(\sigma Z) - \sinh(\sigma Z)\right]\mathscr{W}_0^*, \tag{6.16}$$

where

$$H(\xi) = \xi + \frac{(1+\mathrm{i})D}{2}\left[1 - \mathrm{e}^{-(1-\mathrm{i})\xi}\right]. \tag{6.17}$$

The right sides of (6.15) and (6.16) are the mean Reynolds stresses induced by the leading-order flows and the viscosity inside the bottom boundary layer and the muddy seabed.

https://doi.org/10.1017/jfm.2026.11447 Published online by Cambridge University Press

Physically, it indicates that the mean steady currents arise because a mean shear stress must be presented to balance the Reynolds stress. Beyond the bottom boundary layer, the vertical gradient of $\overline{u}_1$ must vanish because the flow is inviscid in the core region. At the water–seabed interface, the velocity and shear stress are continuous. At the bottom of the seabed, the mean current $\overline{\mathscr{U}}_1$ must be equal to zero to satisfy the no-slip condition. In summary, the boundary conditions for (6.15) and (6.16) can be expressed as

$$\frac{\partial \overline{u}_1}{\partial \xi} = 0, \qquad \xi \to \infty, \tag{6.18}$$

$$\overline{u}_1 = \overline{\mathscr{U}}_1 + \frac{1}{2}\zeta_0^* \left(\frac{A}{d}\frac{\partial \mathscr{U}_0}{\partial Z} - \frac{\epsilon}{\delta_w}\frac{\partial u_0}{\partial \xi} \right), \qquad \xi = 0 \text{ (or } Z = 1), \tag{6.19}$$

$$\frac{\partial \overline{\mathscr{U}}_1}{\partial Z} = \frac{d}{\gamma_m \beta^2 A} \left(\frac{\epsilon}{\delta_w}\frac{\partial \overline{u}_1}{\partial \xi} + \frac{1}{2}\frac{\epsilon^2}{\delta_w^2}\zeta_0^* \frac{\partial^2 u_0}{\partial \xi^2} \right) - \frac{1}{2}\frac{A}{d}\zeta_0^* \frac{\partial^2 \mathscr{U}_0}{\partial Z^2}, \quad \xi = 0 \text{ (or } Z = 1), \tag{6.20}$$

$$\overline{\mathscr{U}}_1 = 0, \qquad Z = 0. \tag{6.21}$$

Note that only the real parts on the right-hand side of (6.15)–(6.21) are to be taken to calculate the second-order steady currents.

Associating with the boundary condition (6.18)–(6.21), $\overline{u}_1$ and $\overline{\mathscr{U}}_1$ can be calculated from (6.15) and (6.16) by integration twice, and the solution can be expressed as

$$\overline{u}_1 = \frac{k_0|\hat{A}|^2}{\sinh^2 q}\mathscr{A}(\xi) + \overline{u}_1|_{\xi=0} = \frac{k_0|\hat{A}|^2}{\sinh^2 q}\left(\mathscr{A}(\xi) + \mathscr{C}_w\right), \tag{6.22}$$

$$\overline{\mathscr{U}}_1 = \frac{k_0|\hat{A}|^2}{\sinh^2 q}\left(\mathscr{C}_m Z - \mathscr{B}(Z)\right). \tag{6.23}$$

The expressions of $\mathscr{A}(\xi)$, $\mathscr{B}(Z)$, $\mathscr{C}_w$ and $\mathscr{C}_m$ are given in Appendix B. As a check, it can be seen that in the limiting cases of $\gamma_m = \beta = 1$, $M_a = 0$ or $d = 0$, (6.22) recovers the Eulerian drift velocity profile within the Stokes boundary layer over a solid plate (Mei *et al.* 2005). At the outer edge of the bottom boundary layer, $\xi \to \infty$, the horizontal component of the steady current velocity can be expressed as

$$\overline{u}_{1\infty} = \overline{u}_1|_{\xi\to\infty} = \frac{k_0|\hat{A}|^2}{\sinh^2 q}\left(\mathscr{A}(\infty) + \mathscr{C}_w\right), \tag{6.24}$$

where

$$\mathscr{A}(\infty) = -\frac{(1-\mathrm{i})D}{2}\frac{\epsilon}{\delta_w}\frac{d}{A}\left(\frac{\mathscr{G}^*(\sigma,\beta)}{\gamma_m} - nM_a^2\tanh^2 q\right) + \mathrm{i}\frac{|D|^2}{2} - D - \frac{|D|^2}{4}. \tag{6.25}$$

For incompressible mud with high viscosity or great elasticity, $M_a = 0$ and $\widehat{d} \to 0$, then $D = -1$ and $\mathscr{G}(\sigma,\beta) \to 0$. In this scenario, the first and second terms on the right-hand side of (6.25) vanish, $\mathscr{C}_w = 0$ and $\overline{u}_{1\infty} = (3/4)(k_0|\hat{A}|^2/\sinh^2 q)$, which is in agreement with the mean Eulerian velocity at the outer edge of the bottom boundary layer over a solid plate (Liu *et al.* 1996).

Because the water–seabed interface is also a material surface, the vertical component of the steady velocity must be equal to zero at the interface and vanishes within the entire bottom boundary layer, that is,

$$\overline{w}_1 = \overline{\mathscr{W}}_1 = 0, \tag{6.26}$$

correct up to $O(\epsilon)$, due to the smallness of the boundary thickness $O(\delta_w)$.

https://doi.org/10.1017/jfm.2026.11447 Published online by Cambridge University Press

In the core region of the water column, the governing equation of the horizontal component of the second-order steady current velocity can be expressed as (Longguet-Higgins 1953; Wen & Liu 1995*a*)

$$\frac{1}{2}\frac{\delta_w^2}{\epsilon^2}\frac{\partial^2\overline{u}_1}{\partial z^2}=\frac{\partial\overline{p}_4}{\partial x}, \tag{6.27}$$

where the mean horizontal pressure gradient is constant and is to be determined by the system condition. Since the steady current is unidirectional and uniform in the x direction, the convection terms do not appear in (6.27). The horizontal component of the steady current velocity in the core region of the water column can be obtained straightforwardly by integrating (6.27) with the boundary conditions at the mean levels of the free surface and the water–seabed interface, (6.12) and (6.24):

$$\overline{u}_1=\frac{\epsilon^2}{\delta_w^2}\frac{\partial\overline{p}_4}{\partial x}\left(z^2-h^2\right)-2k_0^3|\hat{A}|^2(z+h)+\overline{u}_{1\infty}. \tag{6.28}$$

The vertical component of the steady current velocity must vanish in the core region of the water column because $\overline{u}_1$ does not vary with x at both the mean levels of the free surface and the water–seabed interface.

6.3. *Wave-induced mass transport*

During wave propagation, a steady Lagrangian particle velocity, known as the mass transport velocity, is generated within the water column and the muddy seabed (Longguet-Higgins 1953; Ng & Zhang 2007). For flow within the muddy seabed, the mass transport velocity $\mathscr{U}_m$ can be expressed as

$$\mathscr{U}_m=\overline{\mathscr{U}}_1+\overline{\frac{\partial\mathscr{U}_0\mathrm{e}^{\mathrm{i}(k_0x-t)}}{\partial x}\int^t\mathscr{U}_0\mathrm{e}^{\mathrm{i}(k_0x-t)}\,\mathrm{d}t}+\overline{\frac{\partial\mathscr{U}_0\mathrm{e}^{\mathrm{i}(k_0x-t)}}{\partial z}\int^t\mathscr{W}_0\mathrm{e}^{\mathrm{i}(k_0x-t)}\,\mathrm{d}t}, \tag{6.29}$$

where the last two terms on the right-hand side of (6.29) are the velocity components of the Stokes drift. Substituting the leading-order solutions of the horizontal and vertical velocity components of the mud flow, (5.24) and (5.29), into (6.24) yields the Stokes drift velocity:

$$\mathscr{U}_m=\frac{k_0|\hat{A}|^2}{\sinh^2 q}\left[\mathscr{C}_m Z+\mathscr{Q}_1(Z)+\mathscr{Q}_2(Z)-\mathscr{B}(Z)\right]. \tag{6.30}$$

The expressions of $\mathscr{Q}_1(Z)$ and $\mathscr{Q}_2(Z)$ are given in Appendix B.

In the boundary layer adjacent to the water–seabed interface, the mass transport velocity u_m can be written as

$$u_m=\overline{u}_1+\overline{\frac{\partial u_0\mathrm{e}^{\mathrm{i}(k_0x-t)}}{\partial x}\int^t u_0\mathrm{e}^{\mathrm{i}(k_0x-t)}\,\mathrm{d}t}+\overline{\frac{1}{\delta_w}\frac{\partial u_0\mathrm{e}^{\mathrm{i}(k_0x-t)}}{\partial\xi}\int^t w_0\mathrm{e}^{i(k_0x-t)}\,\mathrm{d}t}. \tag{6.31}$$

According to (5.33), (5.36) and (6.22), the mass transport velocity can be determined by

$$u_m=\frac{k_0|\hat{A}|^2}{\sinh^2 q}\left[\mathscr{A}(\xi)+\mathscr{V}_1(\xi)+\mathscr{V}_2(\xi)+\mathscr{C}_m\right], \tag{6.32}$$

where $\mathscr{V}_1(\xi)$ and $\mathscr{V}_2(\xi)$ are given by

https://doi.org/10.1017/jfm.2026.11447 Published online by Cambridge University Press

$$\mathscr{V}_1(\xi) = \frac{1}{2}\left|1 + D\mathrm{e}^{-(1-\mathrm{i})\xi}\right|^2, \tag{6.33}$$

$$\mathscr{V}_2(\xi) = \frac{(\mathrm{i}-1)D}{2}\left\{\left[\xi - D^*\frac{\mathrm{e}^{-(1+\mathrm{i})\xi}-1}{1+\mathrm{i}}\right] - \frac{\epsilon}{\delta_w}\frac{d}{A}\left(nM_a^2\tanh^2 q - \frac{\mathscr{G}^*(\sigma,\beta)}{\gamma_m}\right)\right\}\mathrm{e}^{-(1-\mathrm{i})\xi}. \tag{6.34}$$

When the muddy seabed is incompressible and $\mu \to \infty$, then $\widehat{d} = 0$, $C_1 = 0$, $\overline{u}_1 = 0$ and $D = -1$. Hence, the mass transport velocity within the boundary layer adjacent to the water–seabed interface reduces to

$$u_m = \frac{k_0|\hat{A}|^2}{\sinh^2 q}\left[-\frac{3}{2}\mathrm{e}^{-(1-\mathrm{i})\xi} - \frac{1}{2}\mathrm{e}^{-(1+\mathrm{i})\xi} + \frac{3-2\mathrm{i}}{4}\mathrm{e}^{-2\xi} + \frac{5+2\mathrm{i}}{4}\right], \tag{6.35}$$

and at the outer edge of the boundary layer $\xi \to \infty$,

$$u_m = \frac{5}{4}\frac{k_0|\hat{A}|^2}{\sinh^2 q}, \tag{6.36}$$

which agrees with the well-known solution in the boundary layer adjacent to a horizontal solid bottom obtained by Longguet-Higgins (1953).

In the core region of the water column, the rotational velocity components vanish and the mass transport velocity can be calculated from

$$u_m = \overline{u}_1 + \overline{\frac{\partial \widehat{u}_0 \mathrm{e}^{\mathrm{i}(k_0x-t)}}{\partial x}\int^t \widehat{u}_0\mathrm{e}^{\mathrm{i}(k_0x-t)}\mathrm{d}t} + \overline{\frac{\partial \widehat{u}_0 \mathrm{e}^{\mathrm{i}(k_0x-t)}}{\partial z}\int^t \widehat{w}_0\mathrm{e}^{\mathrm{i}(k_0x-t)}\mathrm{d}t}. \tag{6.37}$$

Substituting the leading-order solution of the inviscid flow, (5.9) and (5.10), and the second-order steady current (6.28) into (6.37), u_m can be expressed as

$$u_m = \frac{\epsilon^2}{\delta_w^2}\frac{\partial \overline{p}_4}{\partial x}\left(z^2 - h^2\right) - 2k_0^3|\hat{A}|^2(z+h) + \overline{u}_{1\infty} + \frac{1}{2}\frac{k_0|\hat{A}|^2}{\sinh^2 q}\cosh(2Q). \tag{6.38}$$

When the system is open and infinitely long in the direction of wave propagation, the mean pressure gradient vanishes in the x direction (Longguet-Higgins 1953; Wen & Liu 1995*b*). In this scenario, the horizontal component of the mass transport velocity becomes

$$u_m = -2k_0^3|\hat{A}|^2(z+h) + \overline{u}_{1\infty} + \frac{1}{2}\frac{k_0|\hat{A}|^2}{\sinh^2 q}\cosh(2Q). \tag{6.39}$$

However, when the system is finite with a closed end, a mean pressure gradient must be present in the x direction to generate a return current, which is to balance the forward steady current so that the net mass flux across the cross-section normal to the direction of wave propagation is zero (Longguet-Higgins 1953), i.e.

$$\int_{-h}^{0} u_m \mathrm{d}z = 0. \tag{6.40}$$

Substituting the general solution (6.38) into (6.40), the pressure gradient in the x direction for a closed system is finally found to be

$$\frac{\partial \overline{p}_4}{\partial x} = \left(\frac{\delta_w}{\epsilon}\right)^2\frac{3}{2h^3}\left(k_0^3|\hat{A}|^2h^2 + \overline{u}_{1\infty}h - \frac{1}{4}\frac{|\hat{A}|^2}{\sinh^2 q}\sinh(2q)\right). \tag{6.41}$$

This spatial gradient of the pressure corresponds to a set-up of the free surface.

https://doi.org/10.1017/jfm.2026.11447 Published online by Cambridge University Press

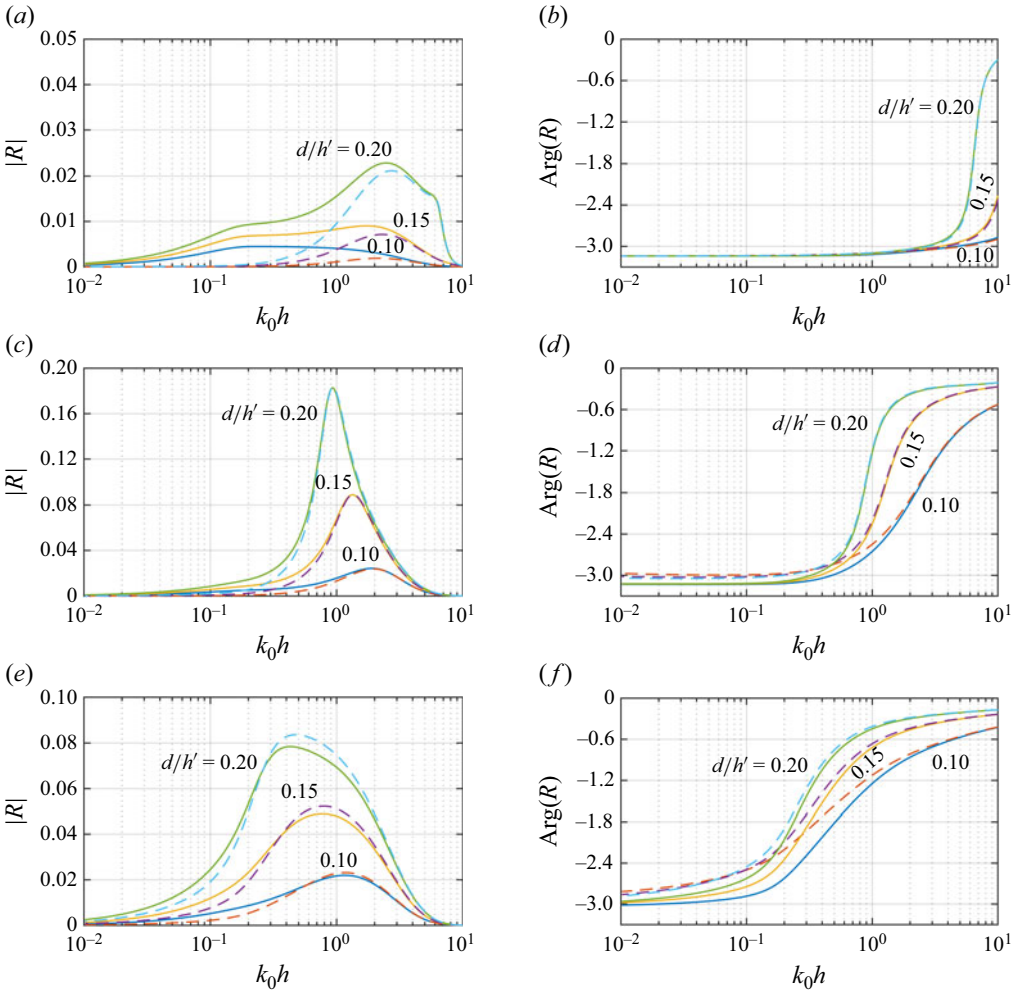


Figure 2. Modulus and phase of the ratios of vertical displacements $R = \epsilon\zeta_0/\eta_0$ in the cases of $d/h' = 0.10$, 0.15 and 0.20. The solid lines are the solution of (7.1) and the dashed lines represent the solution of Mei *et al.* (2010). Results are shown for (*a*,*b*) $G = 20$ kPa, $\mu_m = 10^3$ Pa s; (*c*,*d*) $G = 2.0$ kPa, $\mu_m = 10^3$ Pa s; (*e*,*f*) $G = 0.2$ kPa, $\mu_m = 10^3$ Pa s. The other parameters used in the calculation are given by $h' = 10$ m, $\mu_w = 1$ Pa s, $n = 0.45$, $S_r = 0.90$ and $\gamma_m = 1.91$.

7. Numerical results and discussions

For compressible muddy seabeds, based on (6.7) and (5.38), the ratio of the vertical displacement of the water–seabed interface to that of the free surface can be explicitly written as

$$R = \frac{\epsilon\zeta_0}{\eta_0} = \frac{d}{h'}\frac{q}{\sinh q}\left(\frac{\mathscr{G}(\sigma,\beta)}{\gamma_m} - nM_a^2\tanh^2 q\right). \tag{7.1}$$

Equation (7.1) shows that the vertical displacement of the water–seabed interface is influenced by the compressibility of the seabed. For example, figure 2 illustrates the modulus and phase of the ratios of vertical displacements $R = \epsilon\zeta_0/\eta_0$ for different thicknesses of the muddy seabed, namely $d/h' = 0.10$, 0.15 and 0.20. In the figure, solid lines denote the present solution, while dashed lines correspond to the solution of Mei *et al.*

https://doi.org/10.1017/jfm.2026.11447 Published online by Cambridge University Press

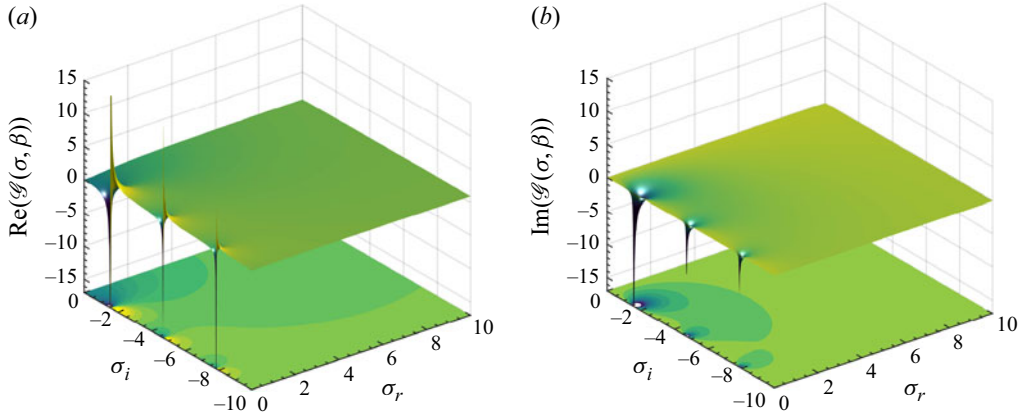


Figure 3. (*a*,*b*) The real and imaginary parts of $\mathscr{G}(\sigma, \beta)$ in the limit where the effective viscosity of mud is significantly greater than that of water, i.e. $\beta \to \infty$.

(2010). As shown in the figure, for a highly elastic muddy seabed, the vertical displacement of the water–seabed interface is significantly underestimated under intermediate and long wave conditions (see figure 2*a*) when the effect of soil compressibility is neglected. In contrast, for a viscous-dominated muddy seabed, an overestimation of the vertical displacement occurs under intermediate wave conditions (see figure 2*e*). In general, a thicker muddy seabed results in larger interface motion, and the water–seabed interface becomes more in phase with the free surface as wavelengths decrease.

In particular, when the effective viscosity of mud is much larger than that of water, β tends to infinity so that

$$F = \tanh\sigma, \ \text{and} \quad \mathscr{G}(\sigma, \beta) = 1 - \frac{\tanh\sigma}{\sigma}. \tag{7.2}$$

Since σ is a complex constant, $\sigma = \sigma_r + \mathrm{i}\sigma_i$, the real and imaginary parts of $\mathscr{G}(\sigma, \beta)$ can be explicitly expressed as

$$\mathrm{Re}(\mathscr{G}(\sigma, \beta)) = 1 - \frac{1}{2|\sigma|^2}\frac{\sigma_r \sinh(2\sigma_r) + \sigma_i \sin(2\sigma_i)}{\sinh^2\sigma_r + \cos^2\sigma_i}, \tag{7.3}$$

$$\mathrm{Im}(\mathscr{G}(\sigma, \beta)) = -\frac{1}{2|\sigma|^2}\frac{\sigma_r \sin(2\sigma_i) - \sigma_i \sinh(2\sigma_r)}{\sinh^2\sigma_r + \cos^2\sigma_i}. \tag{7.4}$$

Clearly, when

$$\sinh\sigma_r = \cos\sigma_i = 0, \tag{7.5}$$

both $\mathrm{Re}(\mathscr{G}(\sigma, \beta))$ and $\mathrm{Im}(\mathscr{G}(\sigma, \beta))$ tend to be infinite, as shown in figure 3. Consequently, $\zeta_0 \to \infty$ becomes significantly larger than the elevation of the free surface, and this substantial amplification indicates the onset of resonance. According to (5.23), (7.5) is satisfied only if

$$\theta = \frac{\pi}{2} \quad \text{and} \quad \widehat{d} = \frac{d}{\delta'_m} = \left(m + \frac{1}{2}\right)\frac{\sqrt{2}\pi}{2}, \quad \text{where } m = 0, 1, 2, \cdots. \tag{7.6}$$

Thus, resonance may occur when the seabed is highly elastic and the ratio of the thickness of the seabed to that of its Stokes' boundary layer equals 1.11, 3.33, 5.55, $\cdots$, for $m = 0, 1, 2, \cdots$, which agrees with the findings of Ng & Zhang (2007) and Mei *et al.* (2010) for incompressible muddy seabeds. Given that $|\mathscr{G}(\sigma, \beta)|$ decays rapidly with increasing

https://doi.org/10.1017/jfm.2026.11447 Published online by Cambridge University Press

$|\sigma|$, only the first few modes are capable of inducing significant resonant responses. It should be noted that when resonance leads to an excessively large amplification, such a case must be regarded as a singular solution within the framework of the present theory, as the underlying assumption of small particle displacement is no longer valid. Moreover, the second-order solutions presented herein are derived under the fundamental assumption of a well-ordered perturbation expansion, which requires the leading-order response to remain finite. Therefore, in the immediate vicinity of the singular points, the present asymptotic formulations for the second-order steady currents and mass transport also become invalid within this narrow parametric regime, where a fully nonlinear analysis would be required for a regularised solution.

Based on (6.7) and (6.8), the elevation of the free surface is also influenced by the compressibility of the seabed soil. Since energy is stored during the compression phase of the seabed and is subsequently released during the expansion phase without dissipation, the relative wave damping rate $\epsilon k_1^i/k_0$ predicted by the present solution matches that derived from Mei *et al.* (2010), as shown in figure 4. However, the fractional phase shift $\epsilon k_1^r/k_0$ is sensitive to the compressibility of the seabed. In figures 4(*a*) and 4(*c*) the sharp decrease in $\epsilon k_1^r/k_0$ corresponds to the onset of resonance. In resonance, the soil undergoes rapid motion, leading to significantly enhanced wave damping, as shown in figures 4(*b*) and 4(*d*). As the seabed thickness increases, the resonant frequencies shift toward shorter wavelengths. Furthermore, with increasing d/h', which amplifies soil motion, both the maximum damping and the associated wavelength increase. We remark here that the present solution is derived under the assumption of $O(d/A) \sim O(1)$. When this scaling is no longer valid, i.e. $O(d) \gg O(A)$, the vertical pore pressure gradient becomes non-negligible and the amplitude of seabed deformation at the water–seabed interface may approach that of the free surface (Tong *et al.* 2026*b*), which may significantly influence the flow dynamics and associated mass transport processes.

Figure 5 presents the vertical profiles of the amplitudes of horizontal and vertical velocity components at leading order within both the muddy seabed and the bottom boundary layer of the water column, under three different compressibility conditions: $M_a = 0$, 0.6 and 1.0. Two typical seabed rheologies are examined: a highly elastic muddy seabed ($G = 5000$ Pa, $\mu_m = 500$ Pa s) and a viscous-dominated muddy seabed ($G = 10$ Pa, $\mu_m = 500$ Pa s). In figure 5 the results for $M_a = 0$ are consistent with the solution of Ng & Zhang (2007) for an incompressible muddy seabed. Owing to its significantly higher effective viscosity μ, the highly elastic seabed exhibits smaller velocity amplitudes, both horizontal and vertical, than those of the viscous-dominated seabed. As shown in figures 5(*a*) and 5(*c*), the profiles of the leading-order horizontal velocity amplitude are identical across all M_a values, confirming that seabed compressibility has no effect on this component. In contrast, seabed compressibility exerts a pronounced and rheology-dependent influence on the vertical velocity amplitude: it increases with M_a in the highly elastic seabed, but decreases with M_a in the viscous-dominated seabed. This opposing trend originates from the fundamental role of seabed rheology in controlling the phase lag between the free surface and the water–seabed interface. Specifically, as the shear modulus G increases from 10 Pa to 5000 Pa, figure 6 shows that the phase difference rises from 0.45 to 3.1 rad, reflecting enhanced resistance to shear deformation and consequent phase lag. Consequently, the time derivative of the pore pressure, $\partial P/\partial t$, exhibits opposite signs in the two seabed types under identical wave forcing. Therefore, when seabed compressibility is non-negligible, (5.18) implies that neglecting compressibility leads to an underestimation of the leading-order vertical velocity in the highly elastic seabed and an overestimation in the viscous-dominated seabed. Because the phase difference between the free surface and the water–seabed interface approaches π for the highly

https://doi.org/10.1017/jfm.2026.11447 Published online by Cambridge University Press

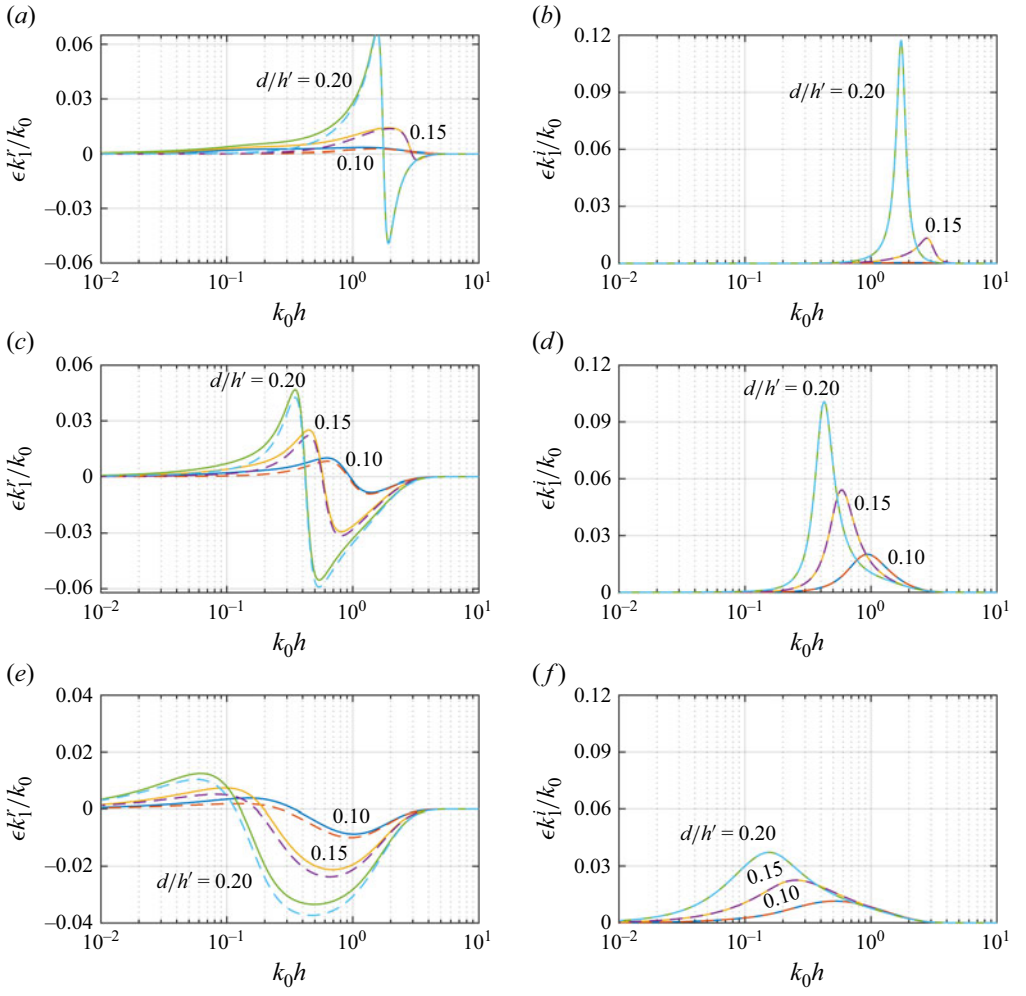


Figure 4. The real and imaginary parts of $\epsilon k_1/k_0$ under the conditions of $d/h' = 0.10$, 0.15 and 0.20. The solid lines are the solution of (7.1) and the dashed lines represent the solution of Mei *et al.* (2010). Results are shown for (*a*,*b*) $G = 5000$ Pa, $\mu_m = 500$ Pa s; (*c*,*d*) $G = 500$ Pa, $\mu_m = 500$ Pa s; (*e*,*f*) $G = 50$ Pa, $\mu_m = 500$ Pa s. The following parameters are used in the calculation: $h' = 10$ m, $\mu_w = 1$Pa s, $n = 0.45$, $S_r = 0.90$ and $\gamma_m = 1.91$.

elastic seabed case, the vertical velocity component undergoes a sign reversal within the bottom boundary layer. Consequently, its amplitude exhibits a non-monotonic profile: decreasing near the interface and then increasing with increasing Z. However, for the viscous-dominated seabed, the vertical velocity amplitude increases monotonically with Z.

The second-order steady current determines the mean discharge rate of mass per unit length across the waves; therefore, it is essential to understand whether this current is affected by the compressibility of the muddy seabed. For clarity, figure 7 presents the vertical profiles of these currents within the bottom boundary layer of the water column and the muddy seabed under conditions of $M_a = 0$, 0.6 and 1.0, respectively. In the figure, the results of $M_a = 0$ correspond to the solution of Ng & Zhang (2007) for an incompressible seabed. The results indicate that $\overline{u}_1$ within the bottom boundary layer

https://doi.org/10.1017/jfm.2026.11447 Published online by Cambridge University Press

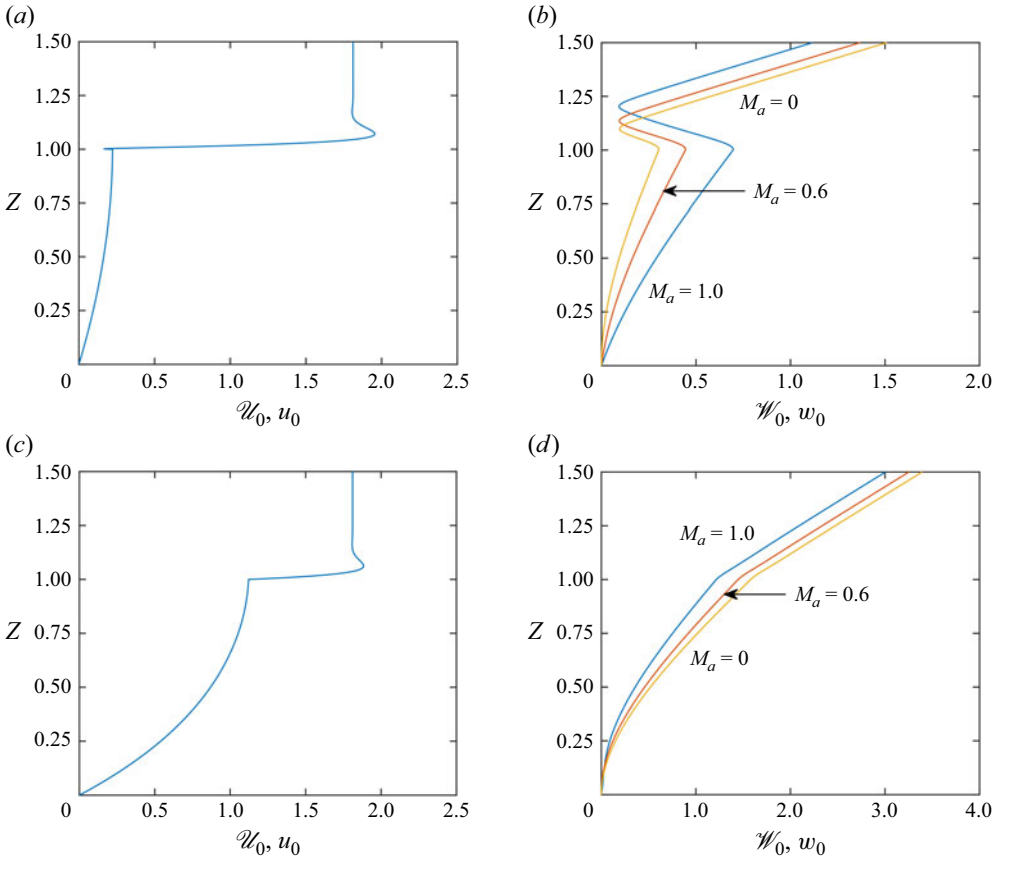


Figure 5. Vertical profiles of the amplitudes of the leading-order velocity components within the bottom boundary layer of the water column and muddy seabeds under various seabed compressibility conditions for (*a*,*b*) a highly elastic muddy seabed with $G = 5000$ Pa and $\mu_m = 500$ Pa s, and (*c*,*d*) a viscous-dominated muddy seabed with $G = 10$ Pa and $\mu_m = 500$ Pa s. In the calculation, $\omega = 0.5$ rad s^{-1}, and the other parameters are given in figure 4.

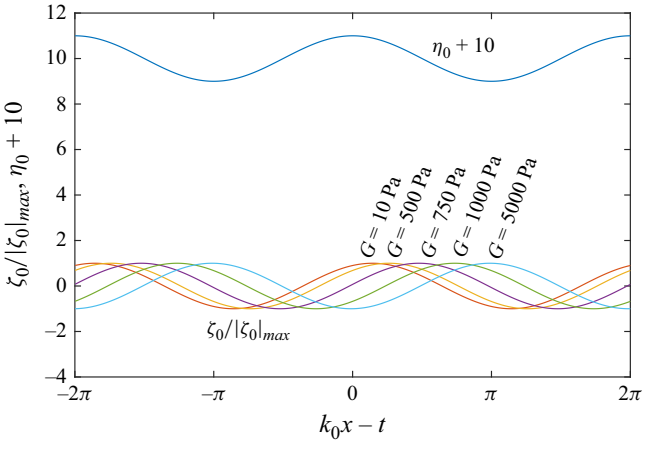


Figure 6. Time histories of the free surface and normalised water–seabed interface under various shear moduli of the seabed. In the calculation, $\mu_m = 500$ Pa s, and the other parameters are given in figure 4.

https://doi.org/10.1017/jfm.2026.11447 Published online by Cambridge University Press

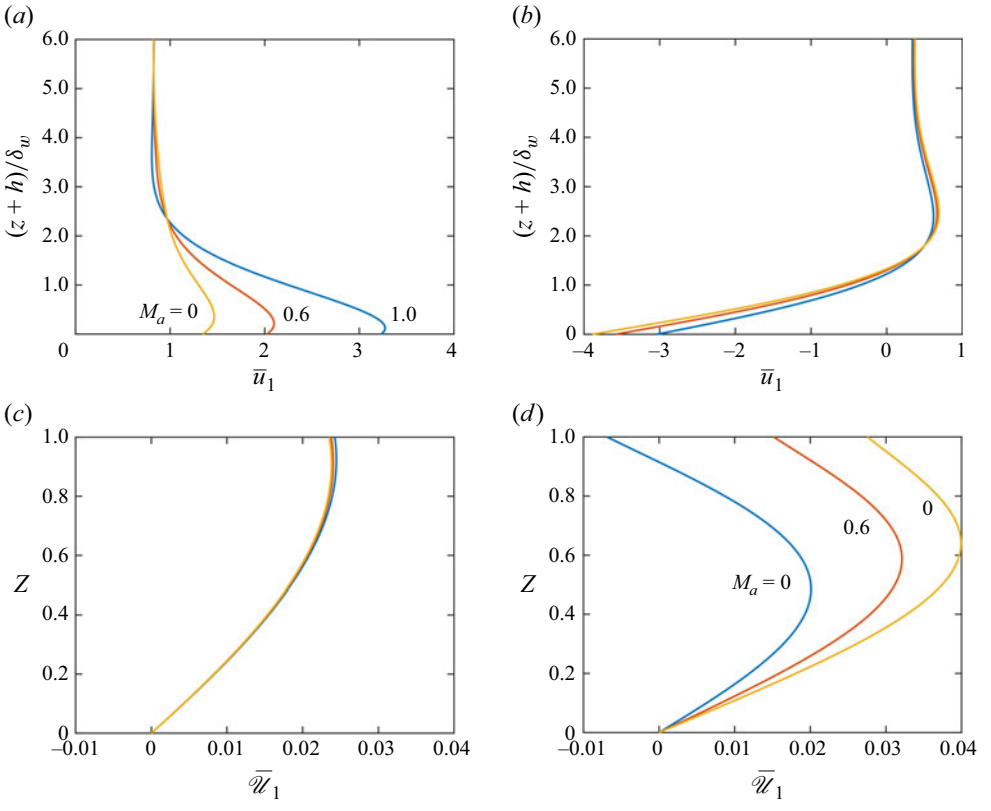


Figure 7. Second-order steady currents within the bottom boundary layer of the water column and muddy seabeds under different seabed compressibility conditions for (*a*,*c*) a highly elastic muddy seabed case with $G = 5000$ Pa and $\mu_m = 500$ Pa s, and (*b*,*d*) a viscous-dominated muddy seabed case with $G = 10$ Pa and $\mu_m = 500$ Pa s. In the figure, δ_w is the thickness of the bottom boundary layer of the water column; the results for $M_a = 0$ correspond to the solution of Ng & Zhang (2007). In the calculation, ω is set to 0.5 rad s^{-1}, and the other parameters are given in figure 4.

above a highly elastic muddy seabed is significantly influenced by the compressibility of the seabed (see figure 7*a*). Overall, it increases with increasing M_a. Neglecting seabed compressibility leads to a 59 % reduction in the second-order steady current at the interface under the condition of $M_a = 1.0$, while the second-order steady current within the muddy seabed, $\overline{\mathscr{U}}_1$, remains nearly unchanged in all cases (see figure 7*c*). In contrast, for a viscous-dominated muddy seabed, the discrepancy between the second-order steady currents within the seabed becomes more pronounced (see figure 7*d*), while the difference in the bottom boundary layer of the water column remains relatively minor, less than 28 %. Given that the seabed thickness is nearly twice that of the bottom boundary layer δ'_m, i.e. $\widehat{d} = 1.95$, the steady current begins to diminish when $Z > 0.6$, leading to a negative value near the interface within the boundary layer. The differences in the second-order steady currents stem predominantly from the dependence of the vertical velocity component on both seabed compressibility and shear stiffness, as previously shown.

Figure 8 further shows the vertical profiles of the mass transport velocity in cases of $M_a = 0$, 0.6 and 1.0, respectively. As expected, the mass transport velocity is continuous across the water–seabed interface. For the highly elastic muddy seabed, mass transport velocities are nearly identical under all three compressibility conditions ($M_a = 0$, 0.6 and

https://doi.org/10.1017/jfm.2026.11447 Published online by Cambridge University Press

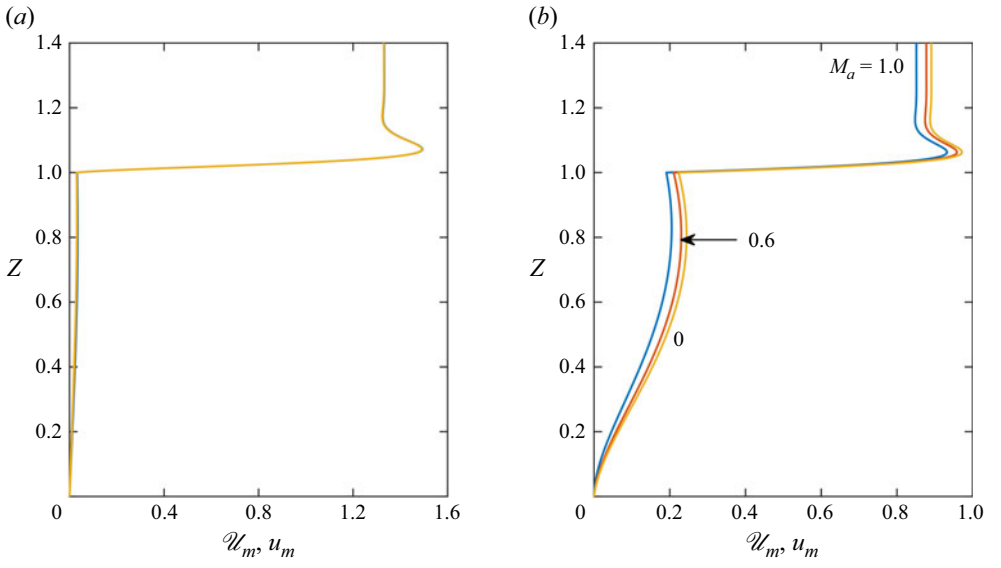


Figure 8. Mass transport velocity within the bottom boundary layer of the water column and muddy seabeds under different seabed compressibility conditions for (*a*) a highly elastic muddy seabed with $G = 5000$ Pa and $\mu_m = 500$ Pa s, and (*b*) a viscous-dominated muddy seabed with $G = 10$ Pa and $\mu_m = 500$ Pa s. In the figure, the results for $M_a = 0$ correspond to the solution of Ng & Zhang (2007). In the calculation, ω is set to 0.5 rad s^{-1}, and the other parameters are given in figure 4.

1.0), owing to its large shear stiffness. In contrast, for the viscous-dominated muddy seabed, some difference exists (see figure 8*b*). At the water–seabed interface, the mass transport velocity for $M_a = 1.0$ is 15 % lower than that of Ng & Zhang (2007) ($M_a = 0$) under the specified wave forcing and mud properties, indicating that neglecting seabed compressibility introduces a systematic overestimation of mass transport in viscous-dominated muddy seabeds. While the entire mud layer undergoes simple shear, the mass transport velocity in water increases upward to a noticeable peak before converging quickly to the limit beyond the boundary layer, consistent with the characteristic behaviour of a single-fluid Stokes boundary layer under progressive waves. As the difference between these two solutions is small beyond the bottom boundary layer, the effect of seabed compressibility on mass transport in the core region of the water column is inconspicuous.

The numerical results presented above clearly demonstrate that the flows within the bottom boundary layer of the water column and the muddy seabed are influenced by the compressibility of the seabed. The explanation for this phenomenon can be summarised as follows. Under identical wave conditions and rheological properties of mud, the leading-order vertical velocity component of mud motion differs between incompressible and compressible muddy seabeds. As a result, the vertical displacement of the water–seabed interface varies under these two bed conditions. For example, when the seabed is compressible, neglecting its compressibility leads to an underestimation of interfacial vertical displacement in highly elastic cases and an overestimation in viscous-dominated cases, as demonstrated previously. The rotational flow within the bottom boundary layer of the water column is sensitive to oscillations of the water–seabed interface (Wen & Liu 1995*b*; Ng 2000). Therefore, Reynolds stress within both the compressible muddy seabed and the bottom boundary layer cannot be accurately predicted using the theory developed for incompressible seabeds. This inaccurate estimation of Reynolds stress ultimately leads

https://doi.org/10.1017/jfm.2026.11447 Published online by Cambridge University Press

to errors in the prediction of second-order steady currents and mass transport velocities during water wave interactions with compressible muddy seabeds.

8. Concluding remarks

In this study, an approximated theory has been developed to investigate water wave propagation over a compressible muddy seabed. Given the relatively small thickness of the wave boundary layer, the core region of the water column is treated as inviscid, and the boundary layer thickness is assumed to be of the same order of magnitude as the wave amplitude. The seabed is assumed to be thin, with its mechanical response under wave loading characterised by a viscoelastic model. The solid skeleton of the mud is considered incompressible, whereas the pore fluid within the seabed is modelled as a compressible medium. Consequently, using a perturbation method, analytical expressions for wave and mud flow are derived at the leading-order boundary value problem, while the evolution of the wave envelope, mean Eulerian velocity and mass transport velocity beneath progressive water waves are obtained at the second order.

Using the present solution, the flow dynamics in the interaction between progressive waves and muddy seabeds is analysed under various seabed conditions and discussed with previous studies of Ng & Zhang (2007) and Mei *et al.* (2010). The results demonstrate that seabed compressibility plays a critical role in modulating the flow both within the bottom boundary layer of the water column and inside the muddy seabed. When compressibility is present, ignoring this effect results in an underestimation of the interface vertical displacement in highly elastic beds and an overestimation in cases dominated by viscous behaviour. The flow in the bottom boundary layer is further modulated by oscillations at the water–seabed interface. As a consequence, the Reynolds stress distributions within the compressible seabed and the overlying boundary layer cannot be accurately described by theories that assume an incompressible seabed. This in turn leads to errors in predicting second-order steady currents and mass transport velocities during wave interactions with compressible muddy seabeds.

In the present study the thickness of the muddy seabed is assumed to be small, and the water wave is purely progressive and propagates in water of intermediate depth. For the case of finite seabed thickness, analysis can be carried out following a similar approach to that of Wen & Liu (1995*b*). If the wave field consists of an incoming wave train and a partially reflected wave train, the interfacial boundary layer problem and mass transport in the core region of the water column can also be addressed, following the methodology of Ng (2004). For long waves in shallow water over a thin compressible muddy seabed, a set of Boussinesq-type equations with the effects of mud flows could be derived in a similar approach to that employed by Liu & Chan (2007*a*). Nevertheless, the conclusions regarding the effects of seabed compressibility on the flow dynamics in water and a muddy seabed would remain similar. Future studies may include large-scale model tests or field observations to improve the understanding of the impact of seabed compressibility on flow dynamics and mass transport. Moreover, although this study establishes the foundational mechanics for monochromatic waves, extension to realistic broad-spectrum sea states, accounting for nonlinear wave interactions and frequency-dependent mud rheology, represents an essential and non-trivial advancement.

Acknowledgements. L.L.T. would like to express his gratitude to Professor Philip L.-F. Liu for warmly hosting his visit to NUS and for providing careful guidance on the research concerning the interaction between waves and the seabed. The authors gratefully acknowledge the comments from the anonymous reviewers, which have significantly contributed to improving the quality of the paper.

https://doi.org/10.1017/jfm.2026.11447 Published online by Cambridge University Press

Funding. L.L.T. is funded by the National Natural Science Foundation of China (52101309). J.S.Z. is funded by Science and Technology Project of China Huaneng Group (HNKJ23-H18).

Declaration of interests. The authors report no conflict of interest.

Author contributions. L.L.T.: conceptualisation, visualisation, methodology, investigation, funding acquisition, formal analysis, writing – original draft. J.S.Z.: project administration, funding acquisition, writing – review & editing. J.H.Z.: formal analysis, writing – review & editing. Y.K.G.: formal analysis, writing – review & editing. N.C.: formal analysis.

Appendix A. Mean Eulerian vorticity in the free surface boundary layer

Since the thickness of the boundary layer is much smaller than the amplitude of the wave, $\epsilon \gg \delta_w$, and the free surface is moving, the following orthogonal curvilinear coordinate system $(\hat{s},\ \hat{n})$ is introduced to describe the flow inside the boundary layer of the free surface:

$$\hat{s} = -x + O(\epsilon), \qquad \hat{n} = -z + O(\epsilon). \tag{A1}$$

Here $\hat{s}$ is tangential to the free surface and $\hat{n}$ is normal to $\hat{s}$ pointing downwards. In terms of curvilinear coordinates, the velocities in the boundary layer can be expressed as

$$u_s = \frac{\partial \psi}{\partial \hat{n}}, \quad w_n = -\frac{1}{\hat{\eta}}\frac{\partial \psi}{\partial \hat{s}}, \tag{A2}$$

where ψ is the streamfunction and $\hat{\eta} = 1 - \hat{n}\kappa$ with κ denoting the curvature of the boundary. In terms of the curvilinear coordinates, the dimensionless governing equation of the motion inside the free surface boundary layer can be written as (Longguet-Higgins 1953)

$$\left[\frac{\partial}{\partial t} + \epsilon\left(\dot{\hat{s}}\frac{\partial}{\partial \hat{s}} + \dot{\hat{n}}\frac{\partial}{\partial \hat{n}}\right)\right]\nabla^2\psi = \frac{\delta_w^2}{2}\frac{\partial^2}{\partial \hat{n}^2}\nabla^2\psi, \tag{A3}$$

where

$$\nabla^2 = \frac{1}{\hat{\eta}}\left[\frac{\partial}{\partial \hat{s}}\left(\frac{1}{\hat{\eta}}\frac{\partial}{\partial \hat{s}}\right) + \frac{\partial}{\partial \hat{n}}\left(\hat{\eta}\frac{\partial}{\partial \hat{n}}\right)\right], \tag{A4}$$

$$\dot{\hat{s}} = \frac{1}{\hat{\eta}}\left(\frac{\partial \hat{\psi}}{\partial \hat{n}} + \hat{n}\Omega\right), \quad \dot{\hat{n}} = -\frac{1}{\hat{\eta}}\frac{\partial \hat{\psi}}{\partial \hat{s}}, \qquad \hat{\psi} = \psi - \psi_b, \tag{A5}$$

with ψ_b and Ω indicating the streamfunction of the free surface motion and the angular velocity of the normal, respectively. Note that κ is of the same order of magnitude as the vertical displacement of the free surface ($O(\epsilon)$) and Ω is of order $O(\epsilon)$ at most (Longguet-Higgins 1953). In terms of ϵ, the streamfunction can be expanded as

$$\psi = \frac{1}{2}\left(\psi_0 + \epsilon\psi_1 + \cdots\right)\mathrm{e}^{-\mathrm{i}(k\hat{s}+t)} + \text{c.c.} \tag{A6}$$

Inside the boundary layer, the tangential derivative of the vorticity is much smaller than its normal derivative. Thus, substituting (A6) into (A3) and retaining the high-order terms, we know that the leading-order vorticity satisfies the following equation:

$$\frac{\delta_w^2}{2}\frac{\partial^2}{\partial \hat{n}^2}\nabla^2\psi_0 + \mathrm{i}\nabla^2\psi_0 = 0. \tag{A7}$$

https://doi.org/10.1017/jfm.2026.11447 Published online by Cambridge University Press

At the outer edge of the boundary layer ($\hat{n}/\delta_w \to \infty$), the vorticity vanishes. At the free surface ($\hat{n} = 0$), the tangential stress vanishes, requiring that

$$\nabla^2 \psi_0 = -2\frac{\partial w_{n0}}{\partial \hat{s}}, \qquad \hat{n} = 0. \tag{A8}$$

The solution of the leading-order vorticity can be readily found as

$$\nabla^2 \psi_0 = -2\frac{\partial w_{n0}}{\partial \hat{s}} \mathrm{e}^{-(1-\mathrm{i})\hat{n}/\delta_w}. \tag{A9}$$

Based on (A3), the next-order governing equation for the boundary layer flow is given by

$$\frac{\partial}{\partial t}\nabla^2 \psi_1 - \frac{\delta_w^2}{2}\frac{\partial^2}{\partial \hat{n}^2}\nabla^2 \psi_1 = -\left(\dot{\hat{s}}\frac{\partial}{\partial \hat{s}} + \dot{\hat{n}}\frac{\partial}{\partial \hat{n}}\right)\nabla^2 \psi_0. \tag{A10}$$

Since the mass transport velocity is steady, taking the average of (A10) over a period yields

$$\frac{\delta_w^2}{2}\frac{\partial^2 \nabla^2 \overline{\psi}_1}{\partial \hat{n}^2} = \overline{\left(\dot{\hat{s}}\frac{\partial}{\partial \hat{s}} + \dot{\hat{n}}\frac{\partial}{\partial \hat{n}}\right)\nabla^2 \psi_0}. \tag{A11}$$

At the free surface, the tangential stress vanishes, therefore, the mean vorticity at the order of $O(\epsilon)$ is given by

$$\nabla^2 \overline{\psi}_1 = -2\kappa_0 \overline{\frac{\partial \psi_0}{\partial \hat{n}}} = -2\overline{\kappa_0 \frac{\partial \psi_0}{\partial \hat{n}}} \quad \text{and} \quad \kappa_0 = -\frac{\partial^2 \eta}{\partial \hat{s}^2}. \tag{A12}$$

Substituting (A5) and (A9) into (A11), the mean vorticity can be calculated by integration, which can be written as

$$\nabla^2 \overline{\psi}_1 = -\mathrm{i}\frac{\partial u_{s0}^*}{\partial \hat{s}}\frac{\partial w_{n0}}{\partial \hat{s}}\left(\lambda \hat{n}\mathrm{e}^{\lambda \hat{n}} - \mathrm{e}^{\lambda \hat{n}} + 2\right), \tag{A13}$$

where

$$\lambda = -\frac{1-\mathrm{i}}{\delta_w}. \tag{A14}$$

Since $\hat{n}$ is approximately vertical and the mean Eulerian drift velocity is constant in parallel to $\hat{s}$, in terms of the Cartesian coordinate system, the mean vorticity can be written as

$$\frac{\partial^2 \overline{\psi}_1}{\partial \hat{n}^2} = k_0^3 |\hat{A}|^2 \left(\lambda \hat{n}\mathrm{e}^{\lambda \hat{n}} - \mathrm{e}^{\lambda \hat{n}} + 2\right). \tag{A15}$$

Note that in (A13) and (A15) only the real part is to be taken into account in the calculation. Beyond the free surface boundary layer, $z/\delta_w \to \infty$, the mean vorticity is independent of viscosity, i.e.

$$\frac{\partial \overline{u}_1}{\partial z} = -2k_0^3 |\hat{A}|^2, \tag{A16}$$

which agrees with the results in Wen & Liu (1995*b*).

Appendix B. Expressions of the terms in the second-order steady current velocities

In the expressions of $\overline{u}_1$ and $\overline{U}_1$, $\mathscr{A}(\xi)$ and $\mathscr{B}(Z)$ are two functions. The expression of $\mathscr{A}(\xi)$ is given by

$$\mathscr{A}(\xi) = \frac{1}{2}C_1\left(\mathrm{e}^{-(1-\mathrm{i})\xi} - 1\right) + \mathrm{i}\mathscr{M}(\xi), \tag{B1}$$

https://doi.org/10.1017/jfm.2026.11447 Published online by Cambridge University Press

where

$$C_1 = (1-\mathrm{i})D\frac{\epsilon}{\delta_w}\frac{d}{A}\left(\frac{\mathscr{G}(\sigma,\beta)}{\gamma_m} - nM_a^2\tanh^2 q\right)^*, \tag{B2}$$

$$\mathscr{N}(\xi) = D\left\{\mathrm{e}^{-(1-\mathrm{i})\xi}\left[-\frac{1+\mathrm{i}}{2}\xi - \frac{D^*}{2} - \mathrm{i}\right] + \frac{D^*}{2} + \mathrm{i} + \frac{\mathrm{i}D^*}{4}\left(1-\mathrm{e}^{-2\xi}\right)\right\}. \tag{B3}$$

At the outer edge of the boundary layer, $\xi \to \infty$,

$$\mathscr{A}(\infty) = -\frac{(1-\mathrm{i})D}{2}\frac{\epsilon}{\delta_w}\frac{d}{A}\left(\frac{\mathscr{G}^*(\sigma,\beta)}{\gamma_m} - nM_a^2\tanh^2 q\right) + \mathrm{i}\frac{|D|^2}{2} - D - \frac{|D|^2}{4}. \tag{B4}$$

The function $\mathscr{B}(Z)$ is defined as

$$\begin{aligned}\mathscr{B}(Z) = {} & \frac{(C_3F^* + C_4)}{\sigma}(F\sinh\sigma - \cosh\sigma)\,Z - \frac{C_4}{\sigma^2}\mathscr{L}(1)Z \\ & + \frac{C_3|F|^2 - (C_3F^* + C_4Z)\mathscr{L}(Z)}{\sigma^2} + \frac{2C_4\,(F\sinh(\sigma Z) - \cosh(\sigma Z) + 1)}{\sigma^3} \\ & - C_3\left[\frac{|F|^2+1}{2}\frac{2\sigma_r Z\sinh(2\sigma_r) - \cosh(2\sigma_r Z) + 1}{4\sigma_r^2}\right. \\ & + \frac{|F|^2-1}{2}\frac{2\sigma_i Z\sin(2\sigma_i) + \cos(2\sigma_i Z) - 1}{4\sigma_i^2} \\ & \left. - F_r\frac{2\sigma_r Z\cosh(2\sigma_r) - \sinh(2\sigma_r Z)}{4\sigma_r^2} - F_i\frac{2\sigma_i Z\cos(2\sigma_i) - \sin(2\sigma_i Z)}{4\sigma_i^2}\right],\end{aligned} \tag{B5}$$

where

$$C_3 = \frac{1}{2}\frac{1}{\gamma_m^2}\frac{\sigma^4}{|\sigma|^2}, \qquad C_4 = \frac{1}{2}\frac{\sigma^3}{\gamma_m^2}\left(nM_a^2\gamma_m\tanh^2 q - 1\right), \tag{B6}$$

and

$$\mathscr{L}(Z) = [F\cosh(\sigma Z) - \sinh(\sigma Z)]. \tag{B7}$$

The constants, $\mathscr{C}_w$ and $\mathscr{C}_m$, are given by

$$\begin{aligned}\mathscr{C}_m = {} & \frac{d}{\gamma_m\beta^2 A}\left[\frac{\epsilon}{\delta_w}\left(C_1\frac{\mathrm{i}-1}{2} + \mathrm{i}C_2\mathscr{M}(0)\right) - \mathrm{i}\frac{\epsilon^2}{\delta_w^2}\frac{Dd}{A}\left(\frac{\mathscr{G}^*(\sigma,\beta)}{\gamma_m} - nM_a^2\tanh^2 q\right)\right] \\ & - \frac{1}{2}\frac{\sigma^2}{\gamma_m}\left(\frac{\mathscr{G}^*(\sigma,\beta)}{\gamma_m} - nM_a^2\tanh^2 q\right)(F\sinh\sigma - \cosh\sigma),\end{aligned} \tag{B8}$$

$$\begin{aligned}\mathscr{C}_w = {} & \mathscr{C}_m - \mathscr{B}(1) + \frac{1}{2}\frac{\sigma}{\gamma_m}\left(\frac{\mathscr{G}^*(\sigma,\beta)}{\gamma_m} - nM_a^2\tanh^2 q\right)(F\cosh\sigma - \sinh\sigma) \\ & + \frac{1-\mathrm{i}}{2}\frac{\epsilon}{\delta_w}\frac{Dd}{A}\left(\frac{\mathscr{G}^*(\sigma,\beta)}{\gamma_m} - nM_a^2\tanh^2 q\right),\end{aligned} \tag{B9}$$

where

$$\mathscr{M}(\xi) = \left[\frac{(1+\mathrm{i})\xi + D^* + \mathrm{i}}{2}\mathrm{e}^{-(1-i)\xi} - \frac{(1-\mathrm{i})D^*\mathrm{e}^{-2\xi}}{4}\right]. \tag{B10}$$

https://doi.org/10.1017/jfm.2026.11447 Published online by Cambridge University Press

The expressions of $\mathscr{Q}_1(Z)$ and $\mathscr{Q}_2(Z)$ are given by

$$\mathscr{Q}_1(Z) = \frac{1}{2\gamma_m^2}\left|1-\cosh(\sigma Z)+F\sinh(\sigma Z)\right|^2, \tag{B11}$$

$$\mathscr{Q}_2(Z) = \frac{\sigma}{2\gamma_m^2}\left[(1-n\gamma_m M_a^2\tanh^2 q)Z+\frac{\mathscr{L}^*(Z)-F^*}{\sigma^*}\right]\mathscr{L}(Z). \tag{B12}$$

References

Abdolali, A., Kadri, U. & Kirby, J.T. 2019 Effect of water compressibility, sea-floor elasticity, and field gravitational potential on tsunami phase speed. *Sci. Rep. UK* **9**, 16874.

Abdolali, A., Kirby, J.T. & Bellotti, G. 2015 Depth-integrated equation for hydro-acoustic waves with bottom damping. *J. Fluid Mech.* **766**, R1.

Batchelor, G.K. 2000 *An Introduction to Fluid Dynamics*. Cambridge University Press.

Baumgarten, A.S. & Kamrin, K. 2019*a* A general constitutive model for dense, fine-particle suspensions validated in many geometries. *Proc. Natl Acad. Sci. USA* **116** (42), 20828–20836.

Baumgarten, A.S. & Kamrin, K. 2019*b* A general fluid-sediment mixture model and constitutive theory validated in many flow regimes. *J. Fluid Mech.* **861**, 721–764.

Bennett, R.H. & Faris, J.R. 1979 Ambient and dynamic pore pressures in fine-grained submarine sediments: Missisippi Delta. *Appl. Ocean Res.* **1**, 115–124.

Chan, I.C. 2022 Theoretical model for nonlinear long waves over a thin viscoelastic muddy seabed. *Mathematics* **10** (15), 2715.

Chan, I.C. & Liu, P.L.-F. 2009 Responses of Bingham-plastic muddy seabed to a surface solitary wave. *J. Fluid Mech.* **618**, 155–180.

Chen, N., Tong, L.L., Zhang, J.S., Chen, H., Peng, J. & Guo, Y.K. 2026 Experimental study of soil liquefaction and wave damping during nonlinear waves and silty seabed interaction. *Ocean Engng* **348**, 123937.

Dalrymple, R.A. & Liu, P.L.-F. 1978 Waves over soft muds: a two layer model. *J. Phys. Oceanogr.* **8**, 1121–1131.

Dore, B.D. 1970 Mass transport in layered fluid systems. *J. Fluid Mech.* **40**, 113–126.

Elgar, S. & Raubenheimer, B. 2008 Wave dissipation by muddy seafloors. *Geophys. Res. Lett.* **35**, L07611.

Gade, H.G. 1958 Effects of a non-rigid, impermeable bottom on plane surface waves in shallow water. *J. Mar. Res.* **16**, 61–82.

Garnier, E.I., Huang, Z.H. & Mei, C.C. 2013 Nonlinear long waves over a muddy beach. *J. Fluid Mech.* **718**, 371–397.

Healy, T., Wang, Y. & Healy, H.-J. 2002 *Muddy Coasts of the World: Processes, Deposits and Function*, 1st edn. Elsiver.

Huang, Z.H. & Huhe, A. 2009 A laboratory study of rheological properties of mudflows in Hangzhou Bay, China. *Intl J. Sedim. Res.* **24**, 410–424.

Ji, Y.M., Tong, L.L., Zhang, J.S., Li, H.R., Chen, H., Guo, Y.K. & Xie, S.P. 2026 Experimental study of the seabed responses induced by a floating column with a heave plate. *Coast. Engng* **206**, 104967.

Jiang, F. & Mehta, A.J. 1995 Mudbanks of the southwest coast of India IV: mud viscoelastic properties. *J. Coastal Res.* **11**, 918–926.

Korde, U.A. 2024 Propagation of underwater wave groups in a compressible ocean coupled with an elastic seafloor. *J. Fluid Mech.* **996**, A18.

Liu, M., Wang, Z.W., Yu, K.Q. & Xu, J.P. 2023 Two distinct types of turbidity currents observed in the Manila Trench, South China Sea. *Commun. Earth Environ.* **4**, 108.

Liu, P.L.-F., Davis, M.H. & Downing, S. 1996 Wave-induced boundary layer flows above and in a permeable bed. *J. Fluid Mech.* **325**, 195–218.

Liu, P.L.-F. & Chan, I.C. 2007*a* On long-wave propagation over a fluid-mud seabed. *J. Fluid Mech.* **579**, 467–480.

Liu, P.L.-F. & Chan, I.C. 2007*b* A note on the effects of a thin visco-elastic mud layer on small amplitude water-wave propagation. *Coast. Engng* **54**, 233–247.

Liu, P.L.-F., Park, Y.S. & Lara, J.L. 2007 Long-wave-induced flows in an unsaturated permeable seabed. *J. Fluid Mech.* **586**, 323–345.

Liu, X.L., Lu, Y., Yu, H.Y., Ma, L.K., Li, X.Y., Li, W.J., Zhang, H. & Bian, C.W. 2022 In-situ observation of storm-induced wave-supported fluid mud occurrence in the subaqueous Yellow River delta. *J. Geophys. Res.: Oceans* **127** (7), e2021JC018190.

https://doi.org/10.1017/jfm.2026.11447 Published online by Cambridge University Press

LONGGUET-HIGGINS, M.S. 1953 Mass transport in water waves. *Phil. Trans. R. Soc. Lond. A* **245**, 535–581.
LONGGUET-HIGGINS, M.S. 1960 Mass transport in the boundary layer at a free oscillating surface. *J. Fluid Mech.* **8**, 293–306.
MAA, J.P.Y. & METHA, A.J. 1990 Soft mud response to water waves. *J. Waterway Port Coast. Ocean Engng ASCE* **116**, 634–650.
MACPHERSON, H. 1980 The attenuation of water waves over a non-rigid bed. *J. Fluid Mech.* **97**, 721–742.
MADSEN, O.S. 1978 Wave-induced pore pressures and effective stresses in a porous bed. *Géotechnique* **28**, 377–393.
MATHEW, J., BABA, M. & KURIAN, N. 1995 Mudbanks of the southwest coast of India I: wave characteristics. *J. Coast. Res.* **11**, 168–178.
MEI, C.C. & FODA, M.A. 1981 Wave-induced responses in a fluid-filled pore-elastic solid with a free surface-a boundary layer theory. *Geophys. J. R. Astron. Soc.* **66**, 597–631.
MEI, C.C., KROTOV, M., HUANG, Z.H. & HUHE, A. 2010 Short and long waves over a muddy seabed. *J. Fluid Mech.* **643**, 33–58.
MEI, C.C. & LIU, K.-F. 1987 A Bingham-plastic model for a muddy seabed under long waves. *J. Geophys. Res.* **92**, 14581–14594.
MEI, C.C. & LIU, P.L.-F. 1973 The damping of surface gravity waves in a bounded liquid. *J. Fluid Mech.* **59**, 239–256.
MEI, C.C., STIASSNIE, M.A. & YUE, D.K.P. 2005 Theory and applications of ocean surface waves. In *Advanced Series on Ocean Engineering* (ed. P.L.-F Liu). World Scientific.
NG, C.O. 2000 Water waves over a muddy bed: a two-layer Stokes' boundary layer model. *Coast. Engng* **40**, 221–242.
NG, C.O. 2004 Mass transport and set-ups due to partial standing surface waves in a two-layer viscous system. *J. Fluid Mech.* **520**, 297–325.
NG, C.O. & ZHANG, X.Y. 2007 Mass transport in water waves over a thin layer of soft viscoelastic mud. *J. Fluid Mech.* **573**, 105–130.
OURIEMI, M., AUSSILIOUS, P. & GUAZZELLI, É. 2009 Sediment dynamics. Part 1. Bed-load transport by laminar shearing flows. *J. Fluid Mech.* **636**, 295–319.
PARK, Y.S. & LIU, P.L.-F. 2010 Oscillatory pipe flows of a yield-stress fluid. *J. Fluid Mech.* **658**, 211–228.
PIEDRA-CUEVA, C. 1993 On the response of a muddy bottom to surface water waves. *J. Hydraul. Res.* **31**, 681–696.
PIEDRA-CUEVA, C. 1995 Drift velocity of spatially decaying waves in a two-layer viscous system. *J. Fluid Mech.* **299**, 217–239.
SAKAKIYAMA, T. & BYKER, E.W. 1989 Mass transport velocity in mud layer due to progressive waves. *J. Waterway Port Coast. Ocean Engng* **115** (5), 614–633.
SAMIKSHA, S.V., VETHAMONY, P., ROGERS, W.E., PEDNEKAR, P.S., BABU, M.T. & DINESHKUMAR, P.K. 2017 Wave energy dissipation due to mudbanks formed off southwest coast of India. *Estuar. Coast. Shelf Sci.* **196**, 387–398.
SI, P.F., SHI, H.B. & YU, X.P. 2019 A general frictional-collisional model for dense granular flows. *Landslides* **16** (3), 485–496.
SONG, Y.P., SUN, Y.F., WANG, Z.H., DU, X., SONG, B.H. & DONG, L.F. 2022 In situ observation of silt seabed pore pressure response to waves in the subaqueous Yellow River delta. *J. Ocean Univ. China* **21**, 1154–1160.
SUMER, B.M. 2014*a* Flow–structure–seabed interactions in coastal and marine environments. *J. Hydraul. Res.* **52**, 1–13.
SUMER, B.M. 2014*b* Liquefaction around marine structures. In *Advanced Series on Ocean Engineering* (ed. P.L.F. Liu). World Scientific.
TALLING, P.J., et al. 2022 Longest sediment flows yet measured show how major rivers connect efficiently to deep sea. *Nat. Commun.* **13**, 4193.
TONG, L.L., HUANG, Z., ZHANG, J.S., CHEN, N., JENG, D.S., ZHAO, S.L. & LI, X.Y. 2026*a* Experimental study of bimodal spectrum wave-induced dynamic responses in a silty seabed. *Coast. Engng* **204**, 104890.
TONG, L.L., JI, Y.M., ZHANG, J.S., CHEN, H., WANG, L.C., XIE, S.P. & GUO, Y.K. 2026*b* Pore pressure responses and seepage flow inside an unsaturated seabed caused by a floating cylinder. *Ocean Engng* **345**, 123865.
TONG, L.L. & LIU, P.L.-F. 2022 Transient wave-induced pore-water-pressure and soil responses in a shallow unsaturated poroelastic seabed. *J. Fluid Mech.* **938**, A36.
TONG, L.L., ZHANG, J.S., ZHAO, J.L., ZHENG, J.H. & GUO, Y.K. 2020 Modelling study of wave damping over a sandy and a silty bed. *Coast. Engng* **161**, 103756.
VERRUIT, A. 1969 Elastic storage of aquifers. In *Flow Through Porous Media* (ed. J.M. DeWiest). Academic Press.

https://doi.org/10.1017/jfm.2026.11447 Published online by Cambridge University Press

WEBER, J.E.H. & GHAFFARI, P. 2023 Wave-induced Lagrangian drift in a porous seabed. *Environ. Fluid Mech.* **23**, 191–203.

WEN, J.G. & LIU, P.L.-F. 1995*a* Mass transport in water waves over an elastic bed. *Proc. R. Soc. A: Math. Phys. Engng Sci.* **450**, 371–390.

WEN, J.G. & LIU, P.L.-F. 1995*b* Mass transport of interfacial waves in a two-layered fluid system. *J. Fluid Mech.* **297**, 231–254.

WINTERWERP, J.C., DE GRAF, R.F., GROENEWEG, J. & LUOJENDIJK, A.P. 2007 Modeling of wave damping at Guyana mud coast. *Coast. Engng* **54**, 249–261.

XU, J.Y. & HUHE, A. 2016 Rheological study of mudflows at Lianyungang in China. *Intl J. Sedim. Res.* **31**, 71–78.

YAMAMOTO, T. 1981 Wave-induced pore pressures and effective stresses in inhomogeneous seabed foundations. *Ocean Engng* **8**, 1–16.

YAMAMOTO, T., KONING, H.K., SELLMEIJER, H. & HIJUM, E.V. 1978 On the response of a poro-elastic bed to water waves. *J. Fluid Mech.* **87**, 193–206.

YAMAMOTO, T., TAKAHASHI, S. & SCHUCKMAN, B. 1983 Physical modeling of sea-seabed interaction. *J. Engng Mech.* **109**, 54–72.

ZARCH, M.K., ZHANG, L., HAERI, S.M. & HE, J. 2025 Classic, modern, and physics-based rheological laws for geophysical granular flows in a landslide hazard chain. *Earth-Sci. Rev.* **269**, 105204.

ZHAO, H.Y., LIN, F., GAO, Y.R., WANG, Z., LI, M., LIU, X., HAN, S. & JENG, D.S. 2026 Effect of clay content on the coupled seabed response and local scour around a free-spanning pipeline under combined waves and currents. *Coast. Engng* **204**, 104910.

ZIEBELL, J.S., FARINA, L. & KOROTOV, S. 2018 Resuspension and transport of fine sediments by waves over a thin viscoelastic mud with erosion. *J. Comput. Appl. Maths* **340**, 745–752.

https://doi.org/10.1017/jfm.2026.11447 Published online by Cambridge University Press